

Decomposition of the Atlantic Multidecadal Variability in a Historical Climate Simulation

IOANA COLFESCU

National Centre for Atmospheric Science, School of Earth and Environment, University of Leeds, Leeds, United Kingdom

EDWIN K. SCHNEIDER

Department of Atmospheric, Oceanic and Earth Sciences, George Mason University, Fairfax, Virginia

(Manuscript received 28 March 2018, in final form 15 January 2020)

ABSTRACT


The Atlantic multidecadal variability (AMV) modulates various climate features worldwide with enormous societal and economic implications, including variations in hurricane activity in the Atlantic, sea level, West African and Indian monsoon rainfall, European climate, and hemispheric-scale surface temperature. Leading hypotheses regarding the nature and origin of AMV focus primarily on its links with oceanic and coupled ocean–atmosphere internal variability, and on its response to external forcing. The role of another possible process, that of atmospheric noise forcing of the ocean, has received less attention. This is addressed here by means of historical coupled simulations and diagnostic experiments, which isolate the influences of external and atmospheric noise forcings. Our findings show that external forcing is an important driver of the simulated AMV. They also demonstrate that weather noise is key in driving the simulated internal AMV in the southern part (0° – 60° N) of the AMV region, and that weather noise forcing is responsible for up to 10%–20% of the multidecadal internal SST variability in some isolated areas of the subpolar gyre region. Ocean dynamics independent from the weather noise forcing is found to be the dominant cause of multidecadal SST in the northern part of the AMV region.

1. Introduction

Predictability of sea surface temperature variability over the Atlantic at decadal time scale [the Atlantic multidecadal variability (AMV)] depends on the mechanisms involved in producing it. The component of the AMV driven by external forcing is predictable to the extent that the natural (e.g., solar variability, volcanic aerosols) or anthropogenic (e.g., industrial greenhouse gas emissions) sources can be predicted (natural) or projected (anthropogenic). The internal AMV component associated with slowly varying internal ocean dynamics or coupled atmosphere–ocean dynamics could be predictable from the initial state of the ocean. The initiation of internal AMV driven by internal atmospheric variability not forced by the SST (hereafter “weather noise”), defined here as the part of the atmospheric variability not produced by external or SST forcing, is expected to be

essentially unpredictable; however, the evolution and decay of an existing AMV event forced by prior weather noise could have predictability involving ocean dynamics and coupled processes. In this regard reliability of future AMV predictions translates into understanding the relative role of these potential drivers.

Atlantic multidecadal variability (Deser and Blackmon 1993; Bjerknes 1964; Schlesinger and Ramankutty 1994; Kushnir and Held 1996; Mann and Park 1996; Enfield et al. 2001; Delworth et al. 2007) is the main mode of multidecadal SST variability observed in the North Atlantic. Estimates from observations made from the late nineteenth century to the present suggest an oscillatory behavior with a 30–70-yr period and a spatial pattern characterized by North Atlantic basinwide fluctuations with a single-signed SST structure. Understanding the mechanisms that are producing AMV are of considerable interest, because AMV is associated with significant climate variability over the continents, including modulation

 Denotes content that is immediately available upon publication as open access.

Corresponding author: Ioana Colfescu, ioana.colfescu@ncas.ac.uk



This article is licensed under a [Creative Commons Attribution 4.0 license](http://creativecommons.org/licenses/by/4.0/) (<http://creativecommons.org/licenses/by/4.0/>).

DOI: 10.1175/JCLI-D-18-0180.1

© 2020 American Meteorological Society

Brought to you by NOAA Central Library | Unauthenticated | Downloaded 01/30/24 02:16 PM UTC

of Atlantic hurricanes (Trenberth and Shea 2006; Knight et al. 2006), surface temperatures, and rainfall [e.g., references in Buckley and Marshall (2016)], as well as ocean sea level (Häkkinen et al. 2013). At the same time, different mechanisms have different implications for potential decadal to multidecadal predictability of the climate variability in these regions (Eade et al. 2014; Zhang et al. 2016; Sutton et al. 2018). Additionally, it is important to attribute AMV to external forcing and/or internal variability because the time scale of anthropogenically forced climate change and the period of AMV are not currently distinguishable from each other due to the short length of the observational record.

To isolate the internal component of the AMV, the externally forced component is removed (Trenberth and Shea 2006; Ting et al. 2009). Otterå et al. (2010) and Bellomo et al. (2018) demonstrate that external forcings, including solar forcing and volcano activity, might be an important modulator of AMV. Booth et al. (2012) makes a case for strong aerosol forcing of AMV. Typically, the external component is estimated as the mean (or common) component of the AMV response across an ensemble of CGCM historical simulations. The CGCM approach is subject to considerable uncertainty, including that associated with the impact of past aerosol variations. Once the response of the AMV to external forcing is found, the internal AMV variability can be estimated as a residual, by subtracting the external component from the total. Marini and Frankignoul (2014) demonstrate the sensitivity of the relationship between the AMOC and the internal component of the AMV to the method used in removing the externally forced SST variability.

Many dynamical studies of internal AMV variability have concentrated on the role of the ocean circulation, especially as represented by the Atlantic meridional overturning circulation (AMOC) and the coupled behavior of the ocean/atmosphere system (e.g., Griffies and Bryan 1997a,b; Delworth and Mann 2000; Latif et al. 2004; Knight et al. 2006). A role for stochastic forcing by weather noise in producing AMV has also been recognized (Delworth 1996; Griffies and Bryan 1997a,b; Delworth and Greatbatch 2000; Clement et al. 2015; Chen et al. 2016). The goal of this study is to isolate the component of the internal AMV produced as a response to the weather noise in a historical CGCM simulation and to quantify the contribution of atmospheric “noise” to the total internal AMV.

Häkkinen et al. (2011) note an association of enhanced atmospheric blocking in the North Atlantic with a positive AMV SST index. The enhanced blocking is associated with heat fluxes into the ocean in phase with the AMV SST, suggesting a positive contribution of blocking to maintaining warm AMV anomalies. The results of

Häkkinen et al. (2011) have been interpreted as evidence that enhanced blocking is forced by a positive phase of the AMV (e.g., Peings and Magnusdottir 2014). However, the enhanced blocking could be a manifestation of weather noise that is forcing the AMV.

The role of weather noise forcing in driving the AMV is controversial. Clement et al. (2015) found that an AGCM coupled to a slab mixed layer ocean produces strong AMV-like SST variability, showing that AMV with a realistic horseshoe structure and the time evolution can be produced by atmospheric surface heat flux variability without ocean dynamics. Zhang et al. (2016) noted that the sign of the surface heat fluxes leading the maximum of the warm phase of the AMV in an ensemble of selected CGCMs is such as to damp AMV SST anomalies, thus lagging SST. This requires that ocean dynamics generate those anomalies. A similar argument was used by Gulev et al. (2013) with regard to the observed AMV. Heat fluxes in the Clement et al. (2015) atmospheric model/slab ocean configuration generate the SST anomalies by construction and therefore must lead SST. Clement et al. (2016) argued that the Zhang et al. (2016) net heat flux test is not conclusive and may be misleading, since for multidecadal time scales the heat storage tendency might be a small residual of much larger and positive and negative high-frequency episodes of the net surface heat flux that cancel out, so that heat flux and SST are essentially in phase on multidecadal time scales. Zhang et al. (2016) also pointed out the role of oceanic teleconnections between the tropical and high-latitude sectors of the AMV region.

This study extends previous work (i.e., Chen et al. 2016) focusing on the role of the weather noise forcing of internal AMV. Chen et al. (2016) decomposed the weather noise forced AMV in a multicentury constant external forcing climate simulation made with the CCSM3 CGCM into the responses from the various components of the weather noise forcing (heat flux, wind stress, and freshwater flux) applied over the World Ocean and only over the Atlantic basin. Here we extend Chen et al. (2016) using the same model by conducting historical (1870–1998) simulations with prescribed external forcing and by decomposing the weather noise forced response of the AMV into the responses driven by weather noise applied globally, only in the southern North Atlantic, and only in the northern North Atlantic.

Chen et al. (2016) found that weather noise wind stress forcing on the ocean circulation is of primary importance for both the AMV in the region of the separated Gulf Stream, and for AMV-associated AMOC variability. The weather noise heat flux is the dominant forcing for AMV in the eastern North Atlantic in that study,

and produces a dynamical as well as a thermodynamic response in the ocean in some regions. In the model used in that study, the heat flux leads and forces internal AMV, while noise-forced ocean dynamics is more important in others.

Hasselmann (1976) was the first to propose the possibility of an essentially random high-frequency process (e.g., weather noise) to drive low-frequency SST variability, using a single point analytical model of slab mixed layer ocean temperature forced by atmospheric heat flux noise, with damping proportional to the temperature. The prescribed noise forcing has a white power spectrum, with amplitude independent of frequency. The temperature response forced by the noise at a given frequency is found to be proportional to the length of time that the forcing is applied, in other words to the inverse frequency. At low enough frequencies the response is limited by the damping. Colfescu and Schneider (2017) described an example of this behavior using a mixed layer depth of 50 m and a damping parameter of $-15 \text{ W m}^2 \text{ K}^{-1}$. They found the power spectrum of the temperature to be the largest at decadal and longer time scales, and the preferred time scales to become longer as the mixed layer depth increases or the damping decreases. This is a much longer time scale than one might expect from a simple scale analysis of the model equation, due to the occurrence of the parameter π in the analytic solution. Appealing to stochastically forced box models of the AMOC (Bryan and Hansen 1995; Griffies and Tziperman 1995), Griffies and Bryan (1997b) described how extending the Hasselmann mechanism to include ocean dynamics can lead to predictability through damped-oscillatory AMV variability involving the AMOC. The approach of Chen et al. (2016) can be viewed as an extension of Delworth and Greatbatch (2000) in that it includes ocean feedbacks on the atmospheric circulation, allowing the forcing of the ocean by weather noise and the response of the atmosphere to the ocean to be distinguished from each other. Below by explicitly isolating and quantifying the weather noise forced AMV component in a coupled historical simulation, we contribute to the evaluation of the arguments made by Zhang et al. (2016) and Clement et al. (2016).

Here, we address several of the above issues by explicitly quantifying the weather noise forced part of the internal component of the variability in a CGCM simulation (Historical1) used as a proxy realization of historical climate variability and AMV. An ensemble of historically forced CGCM simulations is used to estimate the externally forced AMV, which is subtracted from the evolution of the historical realization to estimate the internal component of the AMV. The weather noise in Historical1 is found using an ensemble of AGCMs

forced by the Historical1 SST external forcing evolution. An interactive ensemble (IE) version of the CGCM is then used to examine the AMV response to the weather noise surface flux forcing. The rest of the manuscript is organized as follows. Section 2 describes the three model configurations used (the CGCM ensemble, AGCM ensemble, and interactive ensemble CGCM), the experimental design, which involves simulations with models in each configuration, and the analysis methods. The analysis of the results, discussed in sections 3 and 4, is restricted to decadal and longer time scales and concentrates on the evaluation of the role of weather noise, including weather-noise-forced ocean dynamics, in modulating internal AMV. In section 4, we infer the roles of weather noise heat flux forcing compared to ocean dynamics by applying the equilibrium assumption suggested by Clement et al. (2016) to our results. Conclusions follow in section 5.

2. Model configurations and methodology

a. Model configurations

1) THE CGCM AND AGCM

The CGCM used is the Community Climate System Model version 3 (CCSM3; Collins et al. 2006b). The AGCM, used for the prescribed SST simulations, is the atmospheric component of CCSM3, the Community Atmosphere Model Version 3 (CAM3; Collins et al. 2006a). In both cases, the atmospheric model is run at a T42 horizontal resolution and with 26 vertical levels, with a top at about 2 hPa. The ocean model is run with a horizontal resolution of $1^\circ \times 1^\circ$, and 40 levels in the vertical. This is a lower-resolution version of the model used in CMIP3 (Randall et al. 2007). Magnusdottir et al. (2004) and Deser et al. (2004) used SST-forced simulations with the same AGCM at the same resolution to examine the atmospheric response to SST forcing in the North Atlantic.

2) THE INTERACTIVE ENSEMBLE CGCM

Because of the intrinsic noise from the various physical sources, it is difficult to design controlled experiments to examine the mechanisms for the internal variability in the CGCM. This situation contrasts with the straightforward experimental design used to isolate the roles of the different types of external forcing when this forcing is specified. In the case of external forcing, the responses of the model climate to the various components of external forcing can be isolated, for example, by comparing the model response with chosen components turned on or off.

We take advantage of the weather noise filtering property of the interactive ensemble configuration of

the CGCM, to perform diagnostic experiments to examine the role of weather noise in the associated CGCM. The IE SST still includes the variability due to external forcing, as well as ocean dynamics processes not forced by the weather noise (hereafter “unforced ocean dynamics”), specifically processes internal to the ocean and coupled atmosphere–ocean processes. The weather noise forcing of the ocean and the external forcing are specified in controlled IE experiments. Although the results from the IE are still not reproducible to the extent that the intrinsic ocean variability and coupled atmosphere–ocean variability are not controlled, the experiments are able to attribute the part of the SST variability due to weather noise forcing.

(i) Configuration. The version of the IE used here is the same as used in [Kirtman et al. \(2009\)](#) and [Chen et al. \(2016\)](#), but with historical external forcing “turned on,” as in [Kirtman et al. \(2011\)](#). It is based on the CCSM3 CGCM and includes identical physics and dynamical representations as in the CGCM. The resolutions of the atmospheric and oceanic components are the same as described in [section 2a\(1\)](#). The difference between CCSM3 and IE-CCSM3 is in the coupling between the atmosphere and the other components. This coupling preserves the response of the surface fluxes to the SST but filters out the forcing of the ocean by the atmospheric weather noise surface fluxes.

The IE [schematic in Fig. 1 in [Kirtman et al. \(2005\)](#)] consists of the CCSM3 ocean, land, and sea ice components (one of each) coupled to the ensemble mean of a six-member ensemble of the CCSM3 atmospheric component (referred to as the IE atmospheric component ensemble) through the flux coupler. Each member of the IE atmospheric ensemble is forced by the same SST, derived from the ocean component of the CGCM. The ocean component is forced by the ensemble mean of the surface fluxes from the IE atmospheric ensemble. The atmosphere–ocean coupling is performed once a day, using the fluxes accumulated during the previous day. The land and sea ice components are coupled to the IE atmospheric ensemble every time step, and ensemble mean atmospheric state variables (wind, temperature, moisture) rather than fluxes are provided to the coupler, a choice made for compatibility with the CCSM3 flux coupler. This coupling strongly reduces the magnitude of the variability of the state variables seen by the land and sea ice components in the IE from those in the CGCM.

A common external forcing is applied to each member in the IE atmospheric component ensemble. Each member of the IE atmospheric ensemble is initialized from different initial conditions, producing weather noise in

each that is uncorrelated with the weather noise in the other members. The responses of the atmospheric surface fluxes to the SST are determined as the mean of the fluxes calculated by the IE atmospheric ensemble members and are fed back to the ocean daily. Time-dependent atmospheric weather noise surface fluxes of heat, wind stress, and freshwater, obtained as described below, are added to the IE atmospheric component ensemble mean surface fluxes to force the IE-CGCM ocean component at the surface. Weather noise forcing is not provided to the IE land and sea ice components.

(ii) Interactive ensemble justification. [Barsugli and Battisti \(1998\)](#) generalized the Hasselmann model to both a coupled atmosphere–ocean model setting and an SST-forced atmosphere model, while [Bretherton and Battisti \(2000\)](#) applied the framework to the interpretation of results from AGCMs forced by historical SST. A key finding from the stochastically forced no-ocean-dynamics simplified model studies is that the only situation where weather noise and SST are related is when the SST is forced by the weather noise. Therefore, interpreting an observed association between the atmospheric circulation and SST as the atmosphere being forced by the ocean is potentially misleading. The noise-forced interactive ensemble used here [[section 2a\(2\)](#)] extends Barsugli and Battisti’s framework for the simple stochastically forced coupled model by replacing the simple slab ocean component with the CCSM3 ocean component, the linear damping atmospheric component with the ensemble mean of the CCSM3 atmospheric component [after [Kirtman and Shukla \(2002\)](#)], and the specified stochastic heat flux forcing with specified heat flux, wind stress, and freshwater flux representing the weather noise evolution in a CCSM3 historical simulation [after [Schneider and Fan \(2007\)](#)]. Thus, the IE generalizes the [Hasselmann \(1976\)](#) and [Barsugli and Battisti \(1998\)](#) stochastically forced model framework to include forcing of full ocean dynamics by the specified noise and CGCM-class representation of the atmospheric feedbacks to the SST.

The rationale behind using the IE is the supposition that atmospheric variability can be decomposed in two components: 1) the “forced” response to the external forcing and SST variability and 2) the “unforced” weather noise. Weather noise in each of the IE atmospheric component ensemble members is uncorrelated with the SST and the weather noise in each of the others due to the chaotic evolution of the atmospheric circulations, since each atmospheric ensemble member is started with different initial conditions. However, the SST and externally forced part of the circulation is the same in each member, since each is forced by the same

TABLE 1. CGCM and AGCM ensemble simulations. All simulations are 1870–1998.

Ensemble name	Model	Ensemble members	Forcing
CCSM3 Historical ensemble	CCSM3: coupled CGCM	Historical1 (synthetic observations) + four other ensemble members Historical2–Historical5	CMIP3 1870–1998 external forcing
CAM3 Historical1 ensemble	CAM3: SST-forced AGCM	6 ensemble members	CMIP3 1870–1998 external forcing + Historical1 1870–1998 SST

SST and external forcing (and in this version of the IE, the same land and sea ice conditions).

Since the variance of the average of N realizations of random noise with variance V is V/N , the variance of the weather noise in the ensemble mean surface flux of this version of the IE (six atmosphere ensemble) is $1/6$ of that in an individual ensemble member, assuming the weather noise in each atmospheric ensemble member is statistically identical and white. The ensemble mean flux, which is the SST and externally forced part of the flux, is the same in each individual member, and consequently is unchanged in the ensemble mean. The IE atmospheric component ensemble mean then filters out the weather noise forcing of the ocean due to the atmospheric component ensemble, with some residual noise, while preserving the response to the external forcing and the atmospheric feedback to the SST evolution.

Filtering out the specific noise evolution in the IE preserves the statistical properties of the weather noise that are crucial for maintaining the mean climate, such as horizontal eddy fluxes of heat and momentum, as well as the responses of these statistics to the external forcing and SST. Consider, for example, the zonal mean poleward eddy heat flux in the IE atmospheric component ensemble. The climatological zonal mean eddy heat flux of each member of the ensemble will have essentially the same latitude/height distribution and seasonal evolution. Consequently, this part of the heat flux will not be affected much by the ensemble averaging, and the ensemble mean eddy heat flux will produce climatological cooling in the lower latitudes and warming in the higher latitudes. Generalizing this argument, the ensemble averaging acts effectively as a time-dependent three-dimensional parameterization of the atmospheric response to the evolution and distribution of the SST and external forcing. The IE atmospheric component ensemble mean fluxes can be expected to act to produce a similar climatology to that given by the standard CGCM run with the same external forcing. The IE-CGCM without the specified weather noise forcing can then be thought of as an intermediate coupled model version of the CGCM. Taking the view that the IE atmospheric component is functionally a single atmospheric model,

the IE is energy conserving, as long as the parent CGCM is energy conserving.

Forcing the IE with specified weather noise reinserts this noise into the forcing of the ocean, but in a controlled and deterministic manner. This procedure produces results that are easily interpreted when the SST variability in the IE without this specified forcing is much smaller than that in the CGCM. In that case, the IE response of the SST variability to the specified noise forcing is expected to be essentially deterministic and reproducible.

b. Methodology

1) HISTORICAL ENSEMBLE: THE RESPONSE TO EXTERNAL FORCING

An ensemble of five 129-yr CCSM3 simulations with historical 1870–1998 forcing, denoted the Historical ensemble, was carried out (Table 1; see also Colfescu and Schneider 2017). The purpose of the Historical ensemble is to provide an estimate of the externally forced signal in order to isolate the total internal variability (from all atmospheric and oceanic sources) from the external signal. Each member of the ensemble was forced by the CMIP3 external forcing used in CCSM3 (Meehl et al. 2006). The initial conditions were obtained by choosing five different 1 January restart files from a 500-yr preindustrial control run with external forcing fixed at 1870 levels (archived as run b30.043 as part of the Community Earth System Model database at the National Center for Atmospheric Research). The preindustrial control run appeared to have reached an equilibrium. The simulation denoted Historical1 was chosen for diagnosis with the IE. Daily data for SST, surface fluxes, wind, and freshwater were saved for Historical1 and used to calculating the weather noise surface fluxes.

2) CALCULATION OF THE WEATHER NOISE

The external component of the variability in Historical1 is taken to be the ensemble mean of the CGCM Historical ensemble. The internal component of the Historical1 variability is found by subtracting the external component from full Historical1 output. The atmospheric variability is separated into two components: a component forced by

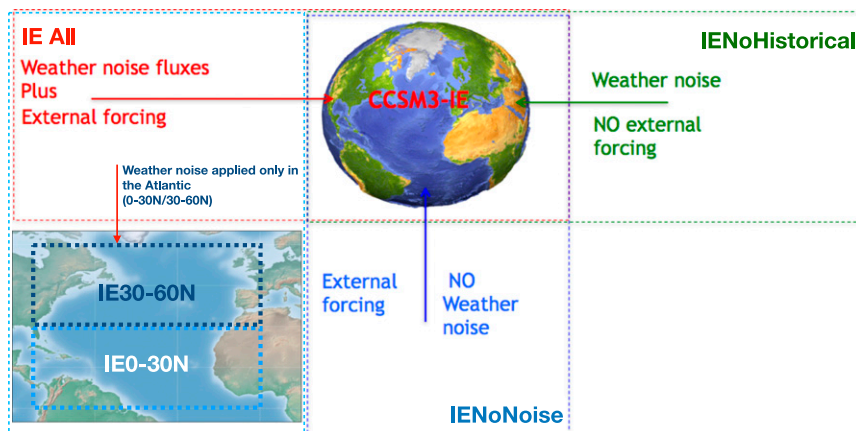


FIG. 1. Interactive ensemble experimental design: IE forced with Historical1 weather noise fluxes and historical external forcing (red); IE forced with Historical1 weather noise fluxes and no external forcing (green); IE forced with historical external forcing and no weather noise fluxes (blue); and regional experiments: IE forced with historical forcing and weather noise fluxes for 0° – 30° and 30° – 60° N for the Atlantic basin (light blue, bottom left corner).

the SST evolution and external forcing (the “forced” component) and the remainder (the “weather noise” component). The forced component is found using a six-member ensemble of CAM3 AGCM simulations, the AGCM Historical1 ensemble. Each ensemble member is forced by the same evolution of Historical1 SST and the same 1870–1998 external forcing as used in the Historical ensemble (Table 1; see also Colfescu and Schneider 2017). Atmospheric initial conditions for each member of the AGCM ensemble differ. The ensemble mean surface fluxes in the AGCM Historical1 ensemble are subtracted from the respective Historical1 surface fluxes to obtain the Historical1 weather noise surface fluxes. The time history of the Historical1 weather noise surface fluxes, including heat flux, wind stress, and freshwater flux components, is used to force the IE ocean component.

Colfescu and Schneider (2017) examined the statistical properties of the EOFs of the surface pressure weather noise in the atmospheric components of two members of the CCSM3 Historical ensemble, one of which is Historical1 in this study. They found the large-scale structures of weather noise to be very similar for both members of the Historical ensemble, and that these structures are also very similar to those in the ensemble members of the respective SST-forced AGCM ensembles corresponding to each of the two coupled runs. The principal component (PC) time series of the EOFs are indistinguishable from white noise for periods longer than 10 years, and the PDFs of the annual mean PC time series are indistinguishable from Gaussian distributions.

Thus, the properties of the Historical1 weather noise appear to fit the stochastic noise assumption for the

weather noise made in the Hasselmann model. The first DJF mode calculated regionally using data restricted to the North Atlantic changes sign at about 50° N and projects strongly on an Arctic Oscillation–like structure (called the “North Atlantic Oscillation” in Schneider and Kinter 1994).

3) INTERACTIVE ENSEMBLE SIMULATIONS

Five IE simulations (Fig. 1; Table 2) were carried out. The purpose of the IE simulations is to quantify the response of the AMV in Historical1 to weather noise surface flux forcing and to compare the AMV responses to weather noise forcing in different regions. Ocean initial conditions were the same as in Historical1. The simulations differ in that the Historical1 weather noise forcing described in section 2b(2) is alternatively applied or switched off, and in that the external forcing is either kept constant at preindustrial conditions or follows the twentieth-century historical values. Internal variability other than that forced by the weather noise is not controlled or suppressed in the IE and is expected to

TABLE 2. Interactive ensemble experiments. All simulations are 1870–1998.

Experiment name	External forcing	Specified atmospheric noise forcing region
IEAll	CMIP3 1870–1998	Global ocean
IENoNoise	CMIP3 1870–1998	None
IENoHistorical	1870 preindustrial	Global ocean
IE0–30N	CMIP3 1870–1998	North Atlantic from 0° to 30° N
IE30–60N	CMIP3 1870–1998	North Atlantic from 30° to 60° N

differ in each simulation. The five IE simulations are described below.

(i) *No weather noise: IENoNoise.* The IENoNoise simulation uses CMIP3 external forcing and no specified weather noise forcing. IENoNoise corresponds to the higher-resolution IE simulation described in [Kirtman et al. \(2011\)](#). In IENoNoise, variability forced by atmospheric weather noise is suppressed, and climate variability is due to external forcing, residual weather noise from incomplete filtering in the IE, and non-weather-noise sources of internal variability. If the weather noise and external forcing are the dominant sources of SST variability, and if biases in the IE climate are small compared to CCSM3, then IENoNoise should approximate the externally forced variability.

(ii) *Global weather noise: IEAll.* The IEAll simulation is forced by prescribed historical external forcing. The Historical1 atmospheric weather noise surface flux forcing is applied over the ice-free parts of the oceans. If internal climate variability in Historical1 is weather noise forced, and if biases in the IE climate are small compared to CCSM3, then the SST variability in IEAll should be close to that in Historical1.

(iii) *Constant external forcing: IENoHistorical.* The IENoHistorical simulation is forced by external forcing set to constant 1870 preindustrial values, using the same settings as in the CCSM3 preindustrial control used for the ocean initial conditions. Historical1 weather noise forcing is applied over the ice-free oceans. IENoHistorical is analogous to the constant external forcing, weather-noise-forced simulation described in [Chen et al. \(2016\)](#). Important differences are that the 129-yr length of the IENoHistorical simulation is the same as the others in [Table 1](#) and uses the same ocean initial state as the other IE simulations, while the simulation in [Chen et al. \(2016\)](#) was carried out for 300 years with 1990 external forcing.

(iv) *Regional weather noise forcing: IE0–30N and IE30–60N.* Two additional simulations were carried out with weather noise forcing applied regionally only over the southern and the northern part of the North Atlantic AMV index region. In IE0–30N, the weather noise forcing was applied only in the North Atlantic between the equator and 30°N, a region mostly inside the North Atlantic subtropical gyre, while in IE30–60N the weather noise forcing was applied only between 30° and 60°N, a region enclosing the North Atlantic subpolar gyre and the northern part of the subtropical gyre.

(v) *The IE bias problem.* The IENoHistorical simulation experiences a noticeable secular cooling in SST, both globally and locally, and does not approach

equilibrium in the 129-yr length of the simulation. The externally forced simulations also have an SST cooling trend compared to the Historical ensemble simulations. The experimental design allows these biases to be partially mitigated in the analysis stage as described in [section 2c](#) and [appendix B](#).

The biases arise because the IE-CCSM3 equilibrium climatology has pronounced biases compared to CCSM3, especially over land and sea ice (Fig. 1b in [Kirtman et al. 2011](#)). The biases in this version of the IE are known to be due to the coupling of the IE atmospheric ensemble to the land and sea ice components using ensemble mean atmospheric fields instead of the net surface fluxes (B. Kirtman 2018, personal communication), a choice that was dictated by the flux coupler architecture of CCSM3 rather than by physical considerations. The biases manifest themselves as a time-dependent drift in the simulations described here, where the ocean initial conditions are taken from the equilibrium climate of a preindustrial constant external forcing CCSM3 simulation. IE-CCSM3 has a cooler preindustrial equilibrium climate than CCSM3; therefore, IENoHistorical started from the CCSM3 equilibrium ocean adjusts to its own equilibrium. The time scale of this adjustment is centennial or longer in the IE simulations. Adjustment due to biases in model climate is a familiar issue when models are used to make decadal time scale initial-value predictions starting from observed initial states (e.g., [Bombardi et al. 2015](#)).

There are also substantial biases in the simulation of multidecadal SST variability by the IE, both external and internal, in the subpolar gyre region of the North Atlantic. As these biases are not eliminated by bias correction and could be a manifestation of the unphysical coupling between the IE atmospheric component ensemble and the sea ice, we cannot unambiguously attribute AMV to weather noise or ocean forcing in that region. Results on the role of ocean dynamics in the subpolar gyre region found from this version of the IE should be considered to be tentative.

c. Analysis

The decomposition of the Historical1 simulation into externally and internally forced components is straightforward. The application of the IE simulations to the decomposition of the internal variability of Historical1 into weather-noise-forced and other sources is in principle also straightforward, but is complicated by the presence of biases in the IE compared to the parent CGCM, and because the internal variability of the IE from sources other than weather forcing has not been filtered out.

1) DECOMPOSITION OF THE SOURCES OF VARIABILITY

The decomposition of the solution from Historical1 into the external and internal components using the Historical ensemble follows Colfescu et al. (2013). This decomposition is given in appendix A. The determination of the weather noise in the Historical1 solution and some of its properties are described in section 2b(2).

The decomposition of a biased solution from the IE into unbiased external and internal components and the estimation of the weather noise forced component of the internal variability are described in appendix B. The bias-corrected internal component of IEAll is given by IEAll minus IENoNoise [Eq. (B4a)]. The bias-corrected external component is given by IEAll minus IENoHistorical [Eq. (B4b)]. The biases removed in the bias correction are given in Eq. (B4c).

We adopt the explained variance E [equivalently correlation squared; Eq. (C1)] as the main metric for quantifying the external and internal components of Historical1 as well as the comparison of the IE and Historical1. Nonphysical noise arises due to the use of small ensembles in the external/internal decompositions, the determination of the weather noise, and the IE responses to the weather noise. The contributions of this “ensembling noise” to the explained variance can be estimated, giving an estimate of the maximum explained variance that could be produced by the weather noise forcing (E_{MAX}) [Eq. (C7)], if the ensemble sizes were large enough so that the ensembling noise was negligible (appendix C). The “ensembling-adjusted explained variance” defined as the ratio E/E_{MAX} provides a rough estimate of the maximum explained variance possible from the physical processes. Statistical significance testing is based on the unadjusted E .

2) INDICES

Global mean SST is calculated from surface temperatures seen by the atmosphere at ocean points, including sea ice points. The monthly values are smoothed using a 132-month running mean filter. The AMV analysis is based on the North Atlantic SST (NASST) index, defined as the monthly mean area average SST over the North Atlantic from the equator to 60°N, over points remaining ice-free for the whole simulation. The AMV index is taken as the annual mean NASST index smoothed by a decadal low-pass Lanczos filter. Compared to using the SST at all ocean points directly from the ocean model, the choice of using SST only from ice-free ocean points has the effect of reducing the amplitude of centennial time scale SST variability in the AMV indices.

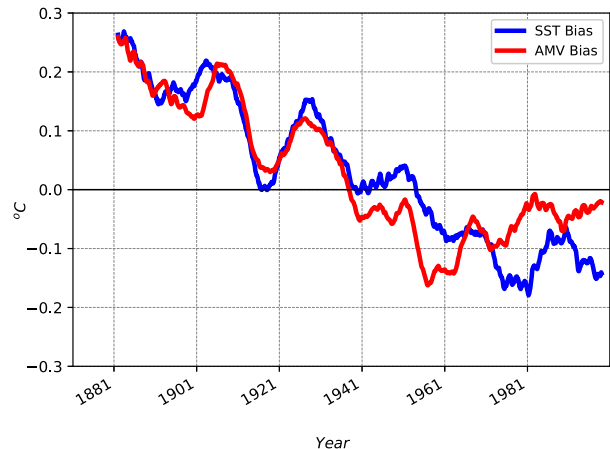


FIG. 2. Time series of annual mean SST index biases from Eq. (C3): Global mean (blue) and North Atlantic AMV region mean (red).

The time series of biases in the 11-yr running mean global mean SST and NASST indices (surface temperature at points with sea ice included for this calculation), calculated from Eq. (B4c), are shown in Fig. 2. Biases in both indices result in a cooling trend of about $0.33^{\circ}\text{C century}^{-1}$ over the period from 1881 to 1998. The biases have noticeable variations around the linear trend on multidecadal time scales, probably since the Int Other variability [see Eq. (B2)] has not been removed. Both biases appear to be leveling off after about 1960.

3. Results

All of the IE results presented in this section refer to the bias-corrected simulations following Eqs. (B4a)–(B4e). The data used in the displayed results (except for those in Fig. 9; power spectra) are low-pass time filtered to remove decadal and shorter periods, in order to isolate the multidecadal and longer period variability. In all of the results presented (except for those in Fig. 4), the external component of Historical1 was computed as the mean of all five members of the Historical ensemble. In the results shown later in Fig. 4, Historical1 was not included in the Historical ensemble mean approximation to the external response to avoid data dependencies. Results shown in figures (other than Fig. 4) are not sensitive to inclusion of Historical1 in the external component ensemble mean.

a. Historical and interactive ensemble global sea surface temperature overview

The global mean SST index is considered first to demonstrate the properties of the external variability of the IE and to provide a context for consideration of the AMV index in section 3b. The decadal filtered global

mean SST and its decomposition into external and internal components for Historical1 and IEAll are shown in Fig. 3. The IE external global mean SST variability is close to the Historical external global mean SST variability (Fig. 3b). The explained variance between the internal components of the global mean SST of Historical1 and IEAll is close to zero, and the variance of the Historical1 internal component is twice that of the IEAll internal component. Weather noise forcing does not explain the internal variability of the global mean SST.

Figures 4a–c show the explained variance E [equivalently correlation squared; Eq. (C1)] of the 10-yr running mean annual mean SST anomalies of the Historical1 variability by the Historical1 external (Fig. 4a) and internal (Fig. 4b) components. At points with sea ice, the temperatures represent the effective surface temperature seen by the atmosphere, which is the area mean of SST over the ice-free portion, ice surface temperature over the ice-covered portion, and land temperatures over the land portion of a grid box. The explained variance of Historical1 by the Historical external component has considerable structure. It is largest in lower latitudes exceeding 0.9 in the tropical Atlantic, Indian, and South Pacific Oceans, and less than 0.1 in much of the North Atlantic between Greenland and Europe as well as in the Southern Ocean. Values are less than 0.3 in the northeastern North Pacific. As might be expected, the explained variance of Historical1 by its internal component is small where the external explained variance is large, especially between 45°S and 40°N, and large where the external explained variance is small. The North Atlantic north of 45°N stands out as the largest region where the Historical1 internal component explained variance is >0.9 . The quantity shown in Fig. 4c is one-half of the sum of the Historical1 external and internal explained variances, where the factor of $\frac{1}{2}$ is chosen so that the same color bar can be used for all of the panels. Where the plotted values are >0.5 , the sum of the external and internal explained variances > 1 , while the sum of explained variances is <1 where the plotted values are <0.5 . As shown in Eq. (C2), departures of this sum from one indicate that the external and internal components are not independent in the sense that they have nonzero covariance. The sense of the dependence is that the external and internal components reinforce where the sum is positive, and partially cancel where the sum is negative. By this measure, the external and internal components are reinforcing in the northern and southern parts of the AMV region, and partially canceling each other in between.

Figure 4d shows the explained variance between the external SST component of Historical1 and the external

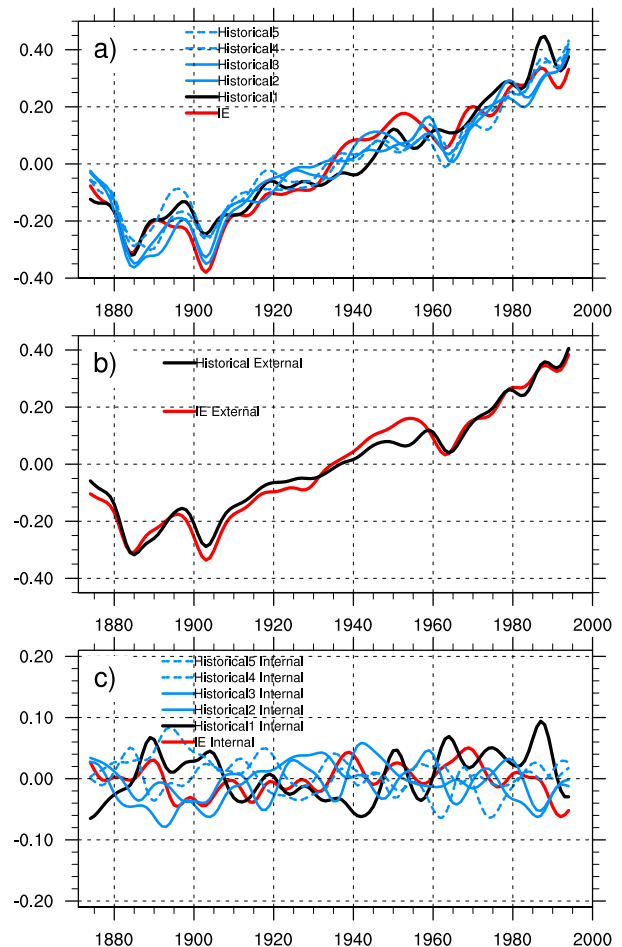


FIG. 3. Global mean SST index ($^{\circ}\text{C}$) for bias-corrected IEAll with global weather noise forcing (red) and Historical simulations: (a) total (Historical1, black; Historical2–5, blue), (b) external components (Historical, black; IEAll, red), and (c) internal components (Historical1, black; Historical2–5, blue; IEAll, red).

component of IEAll. These are generally high, with notable exceptions being the regions of the North Atlantic, North Pacific, and Southern Oceans where the Historical1 external explained variance in Fig. 4a is low. The explained variance between the total SST in Historical1 and IEAll (Fig. 4f) generally has a similar structure to the explained variance between the external component of Historical1 and the external component of IEAll, but with reduced values. An exception to this behavior is in the eastern North Atlantic off the coast of the United States, where the Historical1 external/IEAll external explained variance is >0.8 .

The explained variance of the Historical1 internal component by the IEAll internal component (Fig. 4e) exceeds 0.3 in belts in the tropics and subtropics of the North and South Atlantic, the North Pacific, and the South Indian Oceans, and exceeds 0.5 in the northeastern

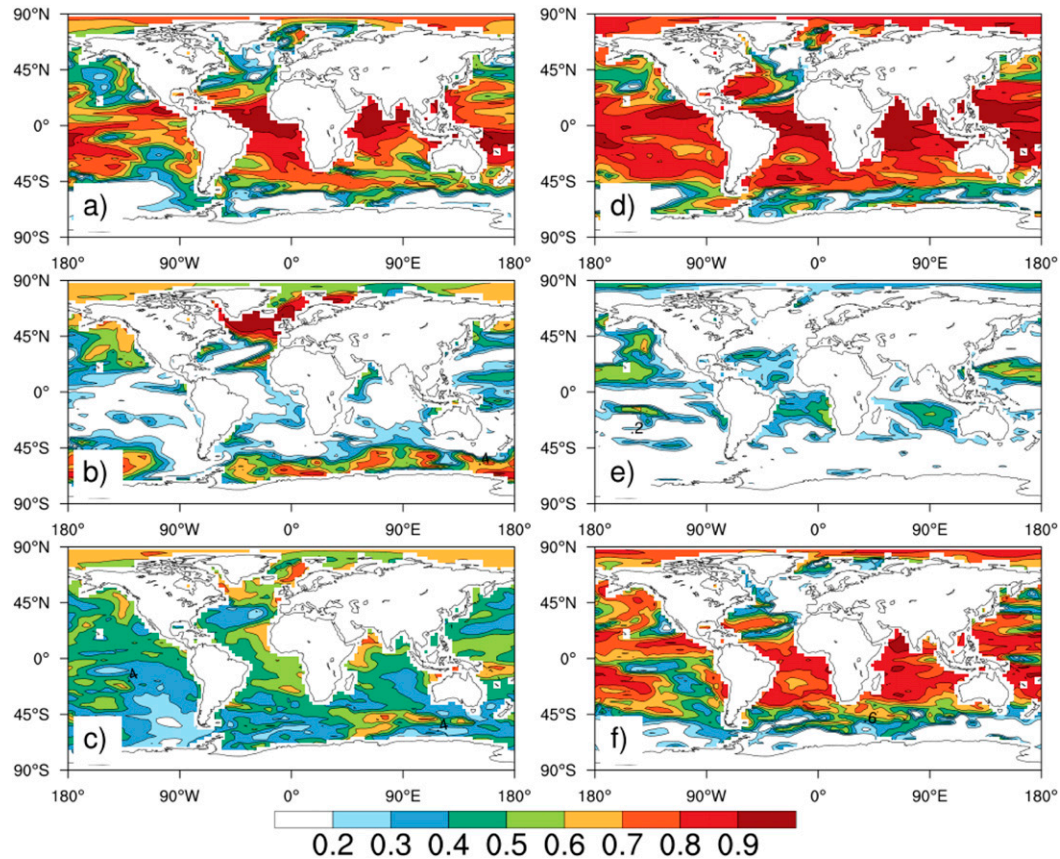


FIG. 4. Point-by-point explained variances (dimensionless) of 10-yr running mean of SST. (left) Explained variances of Historical1 by the Historical1 components: (a) Historical1 total by Historical1 external component, (b) Historical1 total by Historical1 internal component, and (c) $0.5 \times$ the sum of (a) and (b). (right) Explained variances of Historical1 components by bias-corrected IEAll components: (d) Historical1 external by IEAll external, (e) Historical1 internal by IEAll internal (interpreted as the weather-noise-forced contribution), and (f) Historical1 total by IEAll total. Temperatures used over points with sea ice are ocean/sea ice average surface temperatures as seen by the atmosphere.

North Pacific. Notably, the Historical1 internal/IEAll internal explained variance is low in the regions of largest Historical1 internal explained variance in Fig. 4b, the northern North Atlantic and the Southern Ocean. The explained variances are different from zero at the 5% level for $E > 0.13$ using a one-sided t test (since the underlying correlations are positive) and 20 degrees of freedom. Inflation of the Historical1 internal/IEAll internal explained variances using $E_{MAX} = 0.53$ (appendix C; case 1) gives the true Historical1 internal/IEAll internal explained variances potentially >0.9 in regions of the highest explained variance of Fig. 4e. The regions with larger explained variance in Fig. 4e correspond to some extent to the open ocean gyre regions, including the subtropical gyres in all oceans, and the subpolar gyre in the North Pacific, as opposed to the regions with strong ocean currents.

The physical processes potentially involved in the producing substantial explained variance in Fig. 4e are the weather noise forcing, which is the same in Historical1 and IEAll, and the part of the Int Other variability Eqs. (A4) and (B2) associated with unforced ocean dynamics. Internal variability due to unforced ocean dynamics in IEAll and Historical1 is expected to be uncorrelated. Then statistically nonzero explained variance between Historical1 internal and IEAll internal can be attributed to the common weather noise forcing of the two simulations. Weather noise forcing appears to be important for multidecadal internal SST variability in Historical1 throughout much of the subtropics and the northern North Pacific, possibly competitive with unforced ocean dynamics in these regions. On the other hand, the equatorial Pacific, the Southern Ocean, the Kuroshio Extension region and, especially for the main subject of this paper, the

subpolar gyre region of the North Atlantic stand out as regions where weather noise forcing does not explain much of the multidecadal internal SST variability.

b. Atlantic multidecadal variability

The AMV indices for Historical1 and IEAll and their external/internal decompositions are shown in Fig. 5. Internal AMV variances in the Historical ensemble members vary by a factor of 3, with Historical1 having the third largest. The explained variance of the external components of Historical1 and IEAll is 83% and that of the total variability is 57%. The explained variance of the Historical1 internal AMV index by the IEAll internal AMV index is 10% (significant at the 10% level, ensembling-adjusted explained variance 19% with $E_{MAX} = 0.53$), indicating that the weather noise forcing could be making a contribution but is not dominant source of internal AMV variability in Historical1.

The internal AMV index of Historical1 has noticeable quadratic centennial time scale variability with a period too long to be resolved by the 128-yr simulations, warm before 1900 and after 1960 and cold in between. The centennial variability is enhanced when the AMV index is evaluated from the top-layer temperature in the ocean model. This centennial time scale variability is not found in any of the bias-corrected noise-forced IE simulations. Thus, it appears not to be weather noise forced and would be attributed to unforced ocean dynamics. When the centennial variability in the Historical1 internal AMV is filtered out, the explained variance of Historical1 by IEAll is increased to 0.17. The increase is not significant at the 10% level.

The explained variances between the AMV indices of the Historical1 simulation and IE are shown in Fig. 6 (note that the array is symmetric about the top left to lower right diagonal). Higher variances are associated with darker colors, and lower variances with lighter colors. The explained variances between various indices are arranged in “clusters” of similarity (represented by color). For example the highest variance values can be seen in the group comprising indices including external, total, and regional forcing, which are all closely related (darkest blue shades). The IEAll internal is related to internal regional components (IE0–30N internal and IE30–60N). Similarly, the Historical1 internal is related only to the regional simulations (0–30N and 30–60N) as well as Historical1 total and IE. The Historical1 internal/IE internal correlation is not strong, indicating that weather noise forcing may be playing a noticeable role in the forcing the Historical1 AMV but that other processes are more important.

The AMV patterns associated with the various AMV indices, found by regression of the AMV indices with

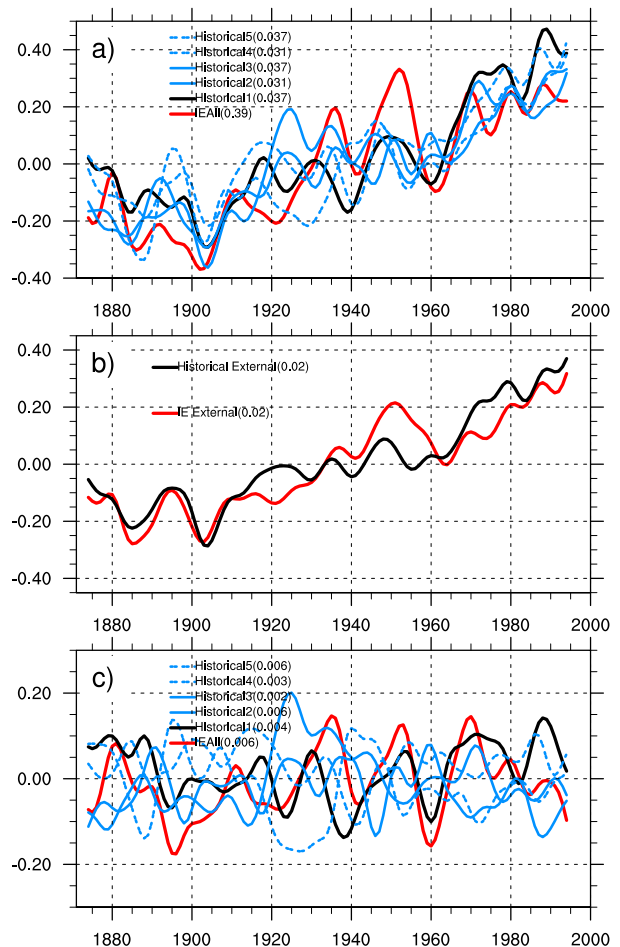


FIG. 5. AMV index anomalies ($^{\circ}\text{C}$) for (a) Historical1 (dark black), Historical2–Historical5 (light blues), and IEAll total (red); (b) Historical external (black) and IE external (red); and (c) as in (a), but for the internal components. Points with sea ice are excluded from the calculations. The numbers in the legend, next to the simulation names, are the variances of the AMV indices ($^{\circ}\text{C}^2$).

the SST anomalies from the associated simulations, are shown in Fig. 7. The Historical1, Historical1 external, IE total, and IE external patterns are similar in that they show single-signed positive anomalies throughout the North Atlantic associated with positive AMV index. The patterns have the lobes of higher values in the northern and southern parts of region, separated by a strip of smaller values extending east-northeastward from about 20°N in the western Atlantic. These four patterns agree in having relative maxima extending eastward from the western Atlantic at about 40°N . The Historical1 total pattern has largest values north of 50°N , a feature absent in IE total or the Historical and IE external patterns. A major discrepancy between the simulation of total AMV in IEAll compared to total Historical1, evident from comparing Figs. 7a and 7d, is a

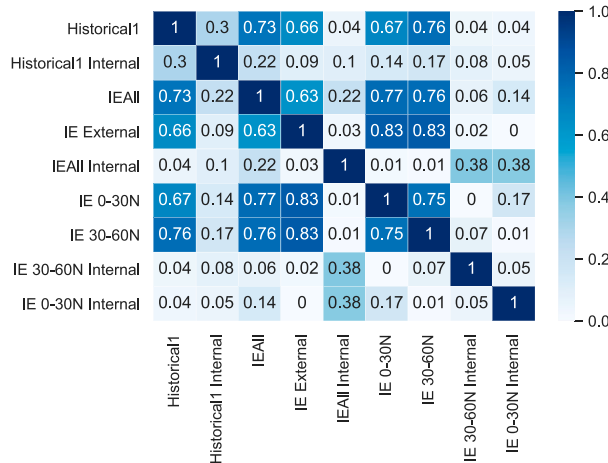


FIG. 6. Variances explained between AMV indices, indicated by numbers in and shading of the boxes.

strong reduction in AMV variance in the subpolar gyre in IEAll. The differences between internal Historical1 (Fig. 7c) and internal IEAll AMV (Fig. 7f) structures in the northern North Atlantic are consistent with the small explained variances between them there in Fig. 4 and the inference of the importance of ocean dynamical processes not involving weather noise forcing in that region.

Using the same models, Chen et al. (2016) found a very similar internal AMV pattern to that shown in Fig. 7f from regressions against multidecadal modes

of the NASST index in both a long constant external forcing run and a weather-noise-forced IE diagnosis of that run. They attributed the largest values in the AMV regression pattern in the central and western North Pacific to forcing by the noise wind stress, and the high values in the eastern North Pacific to forcing by the noise heat flux.

We have examined the AMV patterns from the other four simulations in the Historical ensemble. While the amplitudes of the internal variability patterns in these simulations vary widely and the horseshoe shape is found in only one of them, none of the patterns from the other members of the Historical ensemble have large amplitudes north of 50°N. Historical1 appears to be an outlier in its anomalously strong variability in the northern North Atlantic.

Figure 8 shows power spectra of the AMV indices, computed from annual unfiltered data. The power spectra do not include centennial variability, since periods longer than 64 years are not resolved. The Historical1 and IE total variability spectra have similar structures and amplitudes, and are significantly different from red noise for periods in the 16–20-yr range for Historical1 and 16–22-yr range for IE. The external AMV variabilities in both Historical1 and IE are significantly above red noise for periods longer than 12 years. The Historical1 internal spectrum is above the significance curve for periods from 10 to 24 years and has the largest power of any of the Historical ensemble members in that

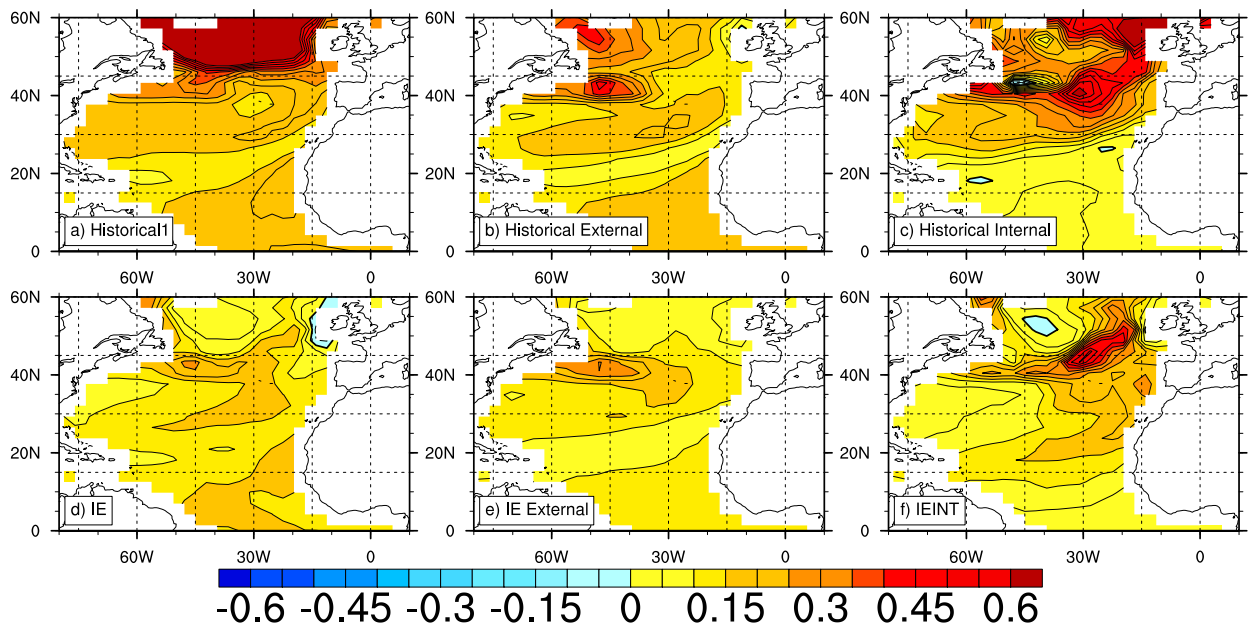


FIG. 7. AMV SST patterns (K per standard deviation) found by regression of standardized AMV total/external/internal indices on total SST anomalies from the respective simulations. The AMV pattern is for (a) Historical1, (b) Historical external, (c) Historical1 internal, (d) IEAll, (e) IE external, and (f) IEAll internal. Points with sea ice are excluded from the calculations.

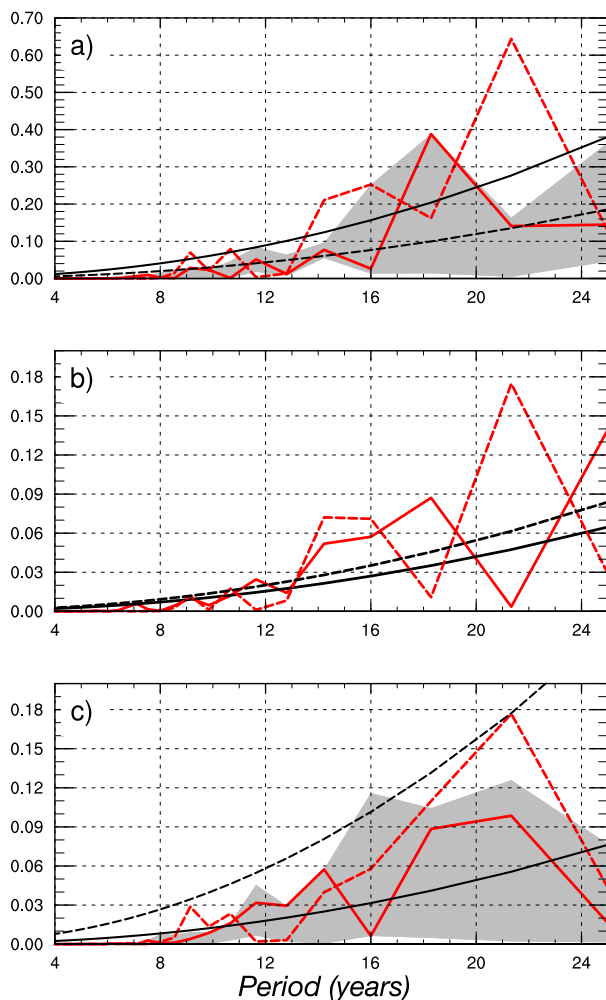


FIG. 8. AMV power spectra for Historical1 (solid red) and IEAll (dotted red): (a) Total, (b) external, and (c) internal. The time series used are unsmoothed detrended annual means. The shading in (a) and (c) represents the spread of the spectra of the individual ensemble members of the Historical ensemble. The black lines represent the 95% confidence level for a red noise Markov test for Historical1 (solid) and IEAll (dotted).

range. All of the Historical ensemble member have significant AMV internal variability in the 15–18-yr range. The 20-yr IE internal spectrum peak is also significantly different from red noise.

Chen et al. (2016) found significant peaks at the 10% confidence level at only 6-, 12- and 100-yr periods in the AMV index of the long constant external forcing simulation.

c. Relationship of AMV and AMOC internal variability

Lag correlations of the internal AMOC against the standardized internal AMV indices in the various Historical and IE simulations are shown in Fig. 9 to give

some indication of the potential role of ocean dynamics in internal AMV. Positive AMOC might be expected to lead positive AMV if the AMOC was responsible for growth of positive AMV anomalies, and negative AMOC might be expected to lead to decay. There are three possible scenarios for ocean dynamics to play a role in internal AMV variability. One is for ocean circulations forced by the weather noise to affect the SST. This process should be simulated by weather-noise-forced IE. The other two mechanisms are for AMV anomalies to be produced by variability of the ocean circulation coupled to the atmosphere, or by ocean circulation variability not coupled to the atmosphere. The latter two mechanisms are possible in the IE, but they would be expected produce variability uncorrelated with that produced by the weather noise forcing, and also uncorrelated between simulations with different forcing or initial conditions.

The most prominent AMOC variability is found at 2-km depth (Fig. 9), but it is not clear how the AMOC structures are related to the forcing of SST internal variability. In Historical1, negative AMOC anomalies at depth with weak surface connection lead AMV. This is opposite in sign to the AMV/AMOC relationship found in Chen et al. (2016). The AMOC–AMV relationship does not have strongly consistent behavior between the Historical simulations, although there is a tendency for positive AMOC anomalies when AMOC leads by 5 and 0 years. Averaging the weighted lag correlations to represent concatenating the time series of the Historical ensemble members produces the Historical average lag regressions (bottom row). In the Historical average, positive AMOC leads AMV and the relationship is strongest at 0 lag. The association collapses when AMV leads AMOC. The Historical average AMV/AMOC regressions resemble those found for the CGCM decadal and multidecadal modes by Chen et al. (2016). The IEAll sequence, which includes both weather-noise-forced and Int Other internal variability, has little similarity to that in Historical1, although possibly some similarity to the historical average, but with the strongest AMOC leading AMV by 5 years. This suggests that there is an AMOC response to the weather noise forcing with enhanced AMOC leading, and decreased AMOC lagging the AMV, that is possibly acting to enhance the AMV variability. However, the strong high-latitude warming found in the structure of the Historical1 AMV does not appear to be explicable as the response to the weather-noise-forced AMOC.

d. Regional noise forcing

The IE0–30N and IE30–60N simulations restrict the weather noise forcing to the southern (0°–30°N) and

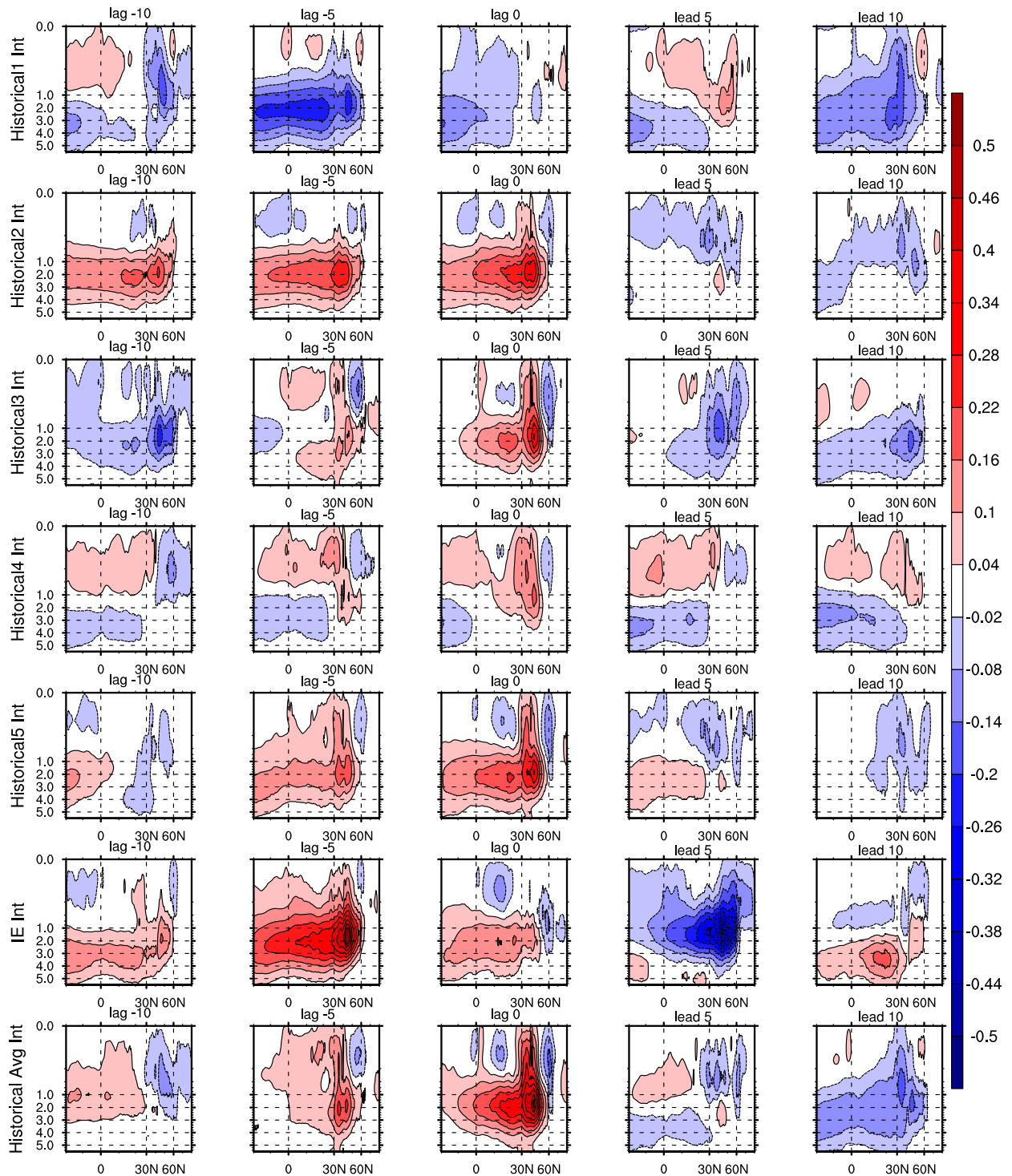


FIG. 9. Lag regressions of standardized AMV internal indices on internal AMOC (Sv per standard deviation; $1 \text{ Sv} \equiv 10^6 \text{ m}^3 \text{ s}^{-1}$) for (first row) Historical1, (second row) Historical2, (third row) Historical3, (fourth row) Historical4, (fifth row) Historical5, (sixth row) IEAll, and (seventh row) Historical average. The time sequences are (left) AMOC leads AMV by 10 years; (center left) AMOC leads by 5 years; (center) simultaneous; (center right) AMOC lags AMV by 5 years; and (right) AMOC lags by 10 years. The vertical scale is depth (km).

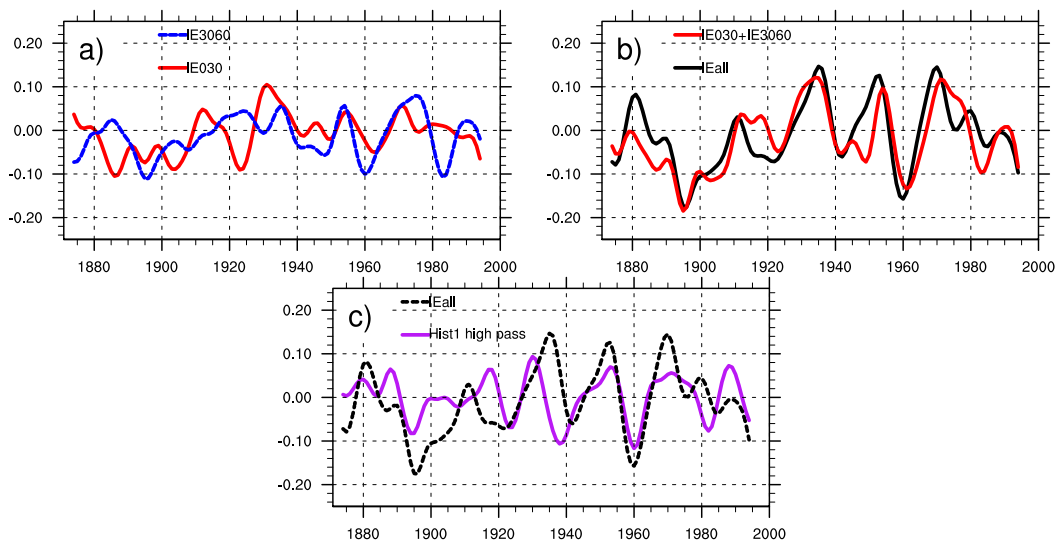


FIG. 10. Internal AMV indices (K): (a) IE30–60N (blue) and IE0–30N (red); (b) sum of IE30–60N and IE0–30N indices (red) and IEAll (black); and (c) Historical1, high-pass filtered to remove centennial time scales (purple) and IEAll (black dotted).

northern (30°–60°N) portions of the AMV region, respectively, with no weather noise forcing outside of these regions. The object of these configurations is to decompose the weather-noise-forced part of the AMV into local and remotely weather-noise-forced components. Figure 10a shows that the internal AMV index responses in IE0–30N and IE30–60N have about the same variance. Their mutual explained variance is 4%. Although weather noise structures can physically connect the weather noise of the two regions (Colfescu and Schneider 2017), the small explained variance indicates this process does not seem to be important with regard to the weather-noise-forced internal AMV index. However, the sum of the AMV index responses in IE0–30N and IE30–60N is a good approximation to the AMV index in IEAll (Fig. 10b), with explained variance 0.63. The internal AMV index in IEAll then can be explained in large part by the combined responses to independent weather noise forcing in the southern and northern parts of the North Atlantic, without appealing to other sources of internal variability.

The top row of Fig. 11 shows the explained variances of the multidecadal internal SST of Historical1 due to the weather noise forcing in various subregions. About 25% (40% ensembling adjusted) of the Historical1 internal SST variance equatorward of 40°N is explained by the global weather noise forcing (Fig. 11a) in IEAll internal. However, the weather-noise-forced explained variance between Historical1 and IEAll is small in the subpolar gyre region. The multidecadal internal SST response to the weather noise forcing appears to be local, with little evidence of influence outside the forcing

region. Weather noise forcing between the equator and 30°N in IE0–30N internal explains part of the internal Historical1 SST response local to that region (Fig. 11b), while the internal Historical1 response to weather noise restricted to the 30°–60°N region in the internal component of IE30–60N internal is also local to that forcing. The explained variance between IE0–30N internal and Historical1 internal SST variability is above 30% (57% ensembling adjusted) in much of the North Atlantic subtropical gyre 0°–30°N region of the noise forcing (Fig. 11b) but small outside the forcing region. The explained variance between IE30–60N internal and Historical1 internal is above 30% in much of the North Atlantic between 30° and 40°N, but small outside of the weather noise forcing region (Fig. 11c). The weather noise forcing apparently does have a minor role in forcing multidecadal variability in the eastern part of the subpolar gyre, with some parts of that region having explained variance between IE30–60N internal and Historical1 internal of 10%–30%. Together, the IE0–30N internal and IE30–60N internal potentially account for much of the noise-adjusted explained variance between IEAll internal and Historical1 internal shown in Fig. 11a. The bulk of the multidecadal SST variability in most of the subpolar gyre appears not to be attributable to weather noise forcing and is then attributed to unforced ocean dynamics.

Quantitative comparison between the results in Figs. 11a–c is highly uncertain. The local weather noise forcing in IE0–30N internal appears to explain more of the internal Historical1 multidecadal SST variance than the global weather noise forcing in IEAll internal.

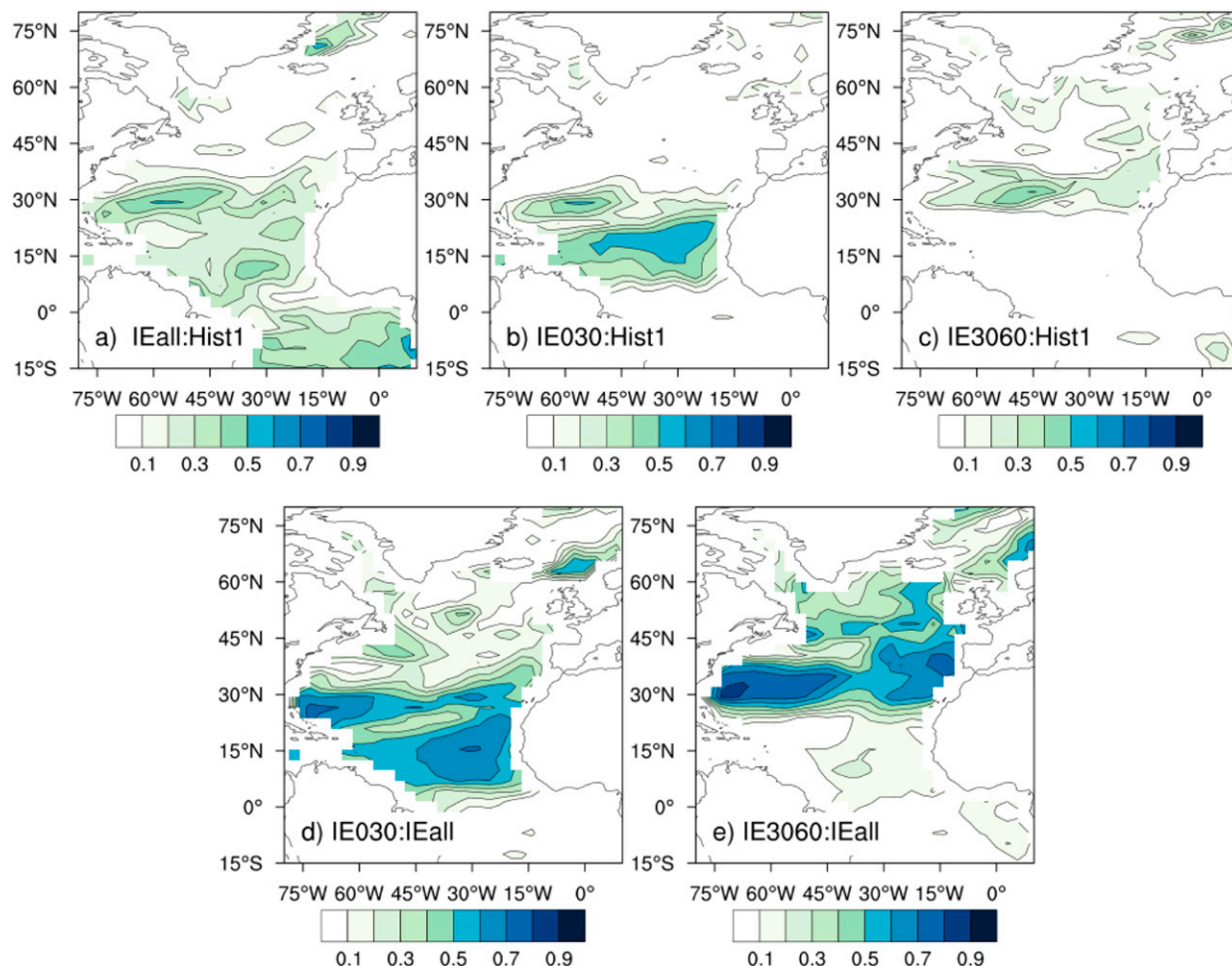


FIG. 11. Explained variances of multidecadal and longer time scale SST variability of (a) Historical1 internal by IEAll internal; (b) Historical1 internal by IE0–30N internal; (c) Historical1 internal by IE30–60N internal; (d) IEAll internal by IE0–30N internal; and (e) IEAll internal by IE30–60N.

However, although the explained variances are significantly different from zero at the 5% level, the differences in the explained variances are not significant at the 10% level (e.g., correlations 0.71 and 0.46 where the difference is largest, at about 53°W and 17°N, using 20 degrees of freedom). Additionally, the explained variances of the full IE simulations (without bias correction or internal/external component separation) with the full Historical1 results are larger between IEAll and Historical1 than between IE0–30N and Historical1 everywhere in the North Atlantic, suggesting that inaccuracies in the estimate of the external component are responsible for the apparent inconsistency.

The bottom row of Fig. 11 shows the explained variances between the multidecadal internal SST of IEAll and the regional IE simulations. The issues addressed in Figs. 11d and 11e are the relationship between the weather-noise-forced responses in the two subregions

and whether unforced ocean dynamics are important for the IE internal SST variability in the subregions. The explained variances become noticeable in the IEAll internal versus regional IE internal cases outside of the common forcing regions. The bias correction is expected to give a background explained variance of about 0.05 when comparing IE simulations in regions where one of the simulations has no weather noise forcing. Explained variances larger than 0.2 in Fig. 11d between 45° and 50°N in the western Atlantic, and in the eastern Atlantic near 15°N in Fig. 11e, are suggestive of possible teleconnections in the response to the weather noise forcing between the northern and southern parts of the AMV region. The small explained internal variances in the subpolar gyre of Historical1 in Fig. 11a or Fig. 11c together with the larger explained variances of IEAll internal by weather noise forcing restricted to the subpolar gyre in Fig. 11e suggest that the multidecadal internal

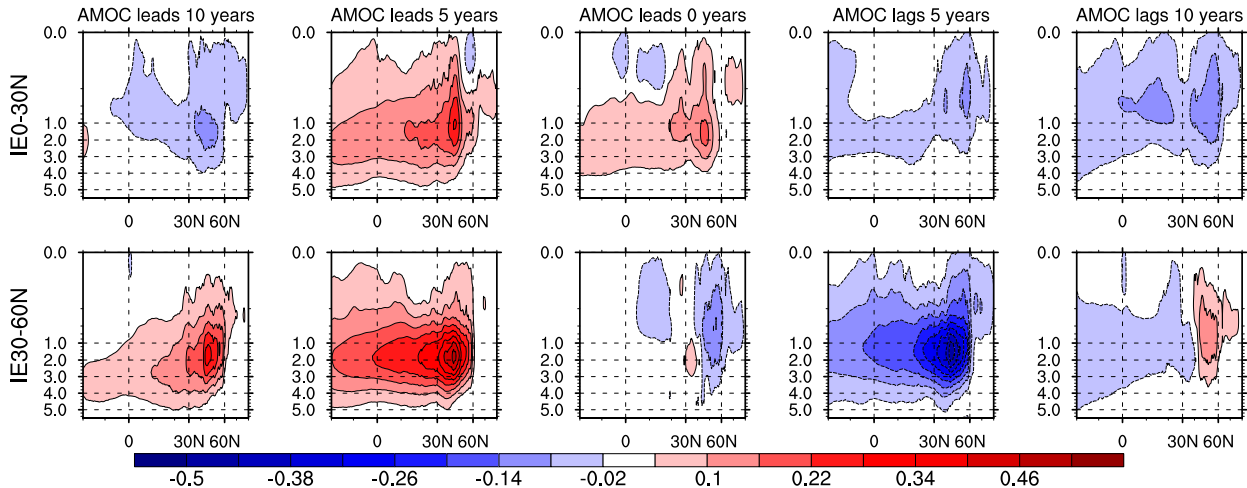


FIG. 12. Internal AMV index lag regressions against internal AMOC as in Fig. 9 for (top) IE0–30N and (bottom) IE30–60N.

SST variability in the subpolar gyre of Historical11 is due to a mechanism not present in the interactive ensemble.

The roles of weather noise forcing in the southern and northern North Atlantic in the AMOC–AMV relationship are shown in Fig. 12. Positive AMOC leads AMV in both IE0–30N and IE30–60N, indicating that AMOC heat fluxes act to enhance AMV growth and decay. The AMOC relationship is stronger in IE30–60N than in IE0–30N and the cell boundary is at the same latitude for both forcings. It is not clear how these differences in AMOC relationship influence the AMV. Since the sum of the AMV indices for IE0–30N and IE30–60N is a good approximation to the IEAll AMV index, the AMOC response in IEAll should be a weighted sum of the AMOC responses of the two regional simulations. Indeed, the AMOC response in IEAll (Fig. 9) resembles that in IE30–60 at most lags, but the response at zero lag resembles that in IE0–30. The weather noise forced AMOC lag regressions in the IE simulations are similar to those found for the multidecadal mode in Chen et al. (2016), who attribute the lag regressions primarily to wind stress forcing, but with a nonnegligible role of the weather noise heat flux. The weather noise forced AMOC response is approximately additive; however, weather noise forcing in either region does not explain the AMV–AMOC relationship simulated in Historical11.

4. Role of ocean dynamics in the simulated AMV

Clement et al. (2016) pointed out that the internal AMV might be expected to be in approximate energy balance due to the long time scale of the variability compared to the decay time scale of the mixed layer

heat content. While this assumption needs to be verified, especially in the regions of deep mixing in the subpolar gyre, it allows us to evaluate the role of ocean dynamics (including the weather-noise-forced ocean dynamics components) compared to that of the weather noise heat flux forcing in the internal AMV found in the Historical11 and IE-CCSM3 simulations.

The point-by-point internal energy budget of the active upper layer of the ocean is

$$dH/dt = A - D, \quad (1)$$

where the net internal surface heat flux from the atmosphere into the ocean A is balanced by the vertically integrated internal ocean heat flux divergence D plus the tendency of the internal ocean heat content vertically integrated over the active layer, dH/dt . The equilibrium energy budget assumption $dH/dt = 0$ then yields from Eq. (1)

$$A = D, \quad (2)$$

so that the ocean dynamics contribution to the heat budget is equal to the net surface heat flux. The decomposition of the net atmospheric heat flux into the weather noise N and feedback/response F components is

$$A = N + F, \quad (3)$$

so that

$$F = D - N. \quad (4)$$

The equilibrium SST results from Eq. (4), as F is a function of SST. The two limiting cases of interest of Eq. (4) are the slab mixed layer balance, where feedback

balances noise heat flux with net surface heat flux and ocean dynamics terms being zero:

$$F = -N, \quad (5)$$

and the ocean dynamics dominant case, where the ocean dynamics term balances the feedback and the weather noise surface heat flux is zero:

$$F = D. \quad (6)$$

The feedback heat flux might be represented as linear damping of SST, $F = -\lambda \times \text{SST}$, with $\lambda > 0$ representing damping or negative feedback (Park et al. 2005). In that case, the SST is given by $\text{SST} = (N - A)/\lambda$. Here, on the other hand, we obtain F from Eq. (4) without assuming a functional form, as the terms on the rhs are known from the simulations: $D = A$ is the net surface heat flux and N is the diagnosed weather noise surface heat flux.

In the energy balance limit in a slab mixed layer configuration, $\text{SST} = N/\lambda$ will be in phase with N . For the 0D model with 50-m mixed layer depth and $\lambda = 15 \text{ W m}^{-2} \text{ K}^{-1}$, the energy balance regime is found for periods longer than about 7–10 years (Colfescu and Schneider 2017). However, in a realistic model, atmospheric teleconnections forced by remote SST anomalies could also contribute to F . When $D \neq 0$ and $|F| \gg |dH/dt|$, the SST is determined by $F = D - N$ and the relative importance of D and N in forcing the SST can be seen by examining the distributions D and N at each point.

Equation (4) is applied to determine F for the Historical1 and the IE simulations, using the internal components of the net surface heat flux from the ocean component output as D and the weather noise net surface heat flux from Historical1 for N . Figure 13 shows the simultaneous regressions of the internal AMV indices of Historical1, IEAll, IE0–30N, and IE30–60N with the 11-yr running mean N , F , and A for the respective simulations. The heat flux regressions are superimposed on the associated internal AMV index/internal SST regressions. The simultaneous lag results are representative of the results out to decadal lead/lag times, as would be expected in the energy balance limit. Several features are apparent in Fig. 13:

- 1) The term F is locally strongly negatively correlated with the internal AMV SST anomalies. The feedback parameter λ is estimated as $20 \text{ W m}^{-2} \text{ K}^{-1}$ with uncertainty of about 50% in Historical1 and the IE simulations.
- 2) South of about 30°N, $N + F \cong 0$, so that the internal AMV SST variability there is driven by N and D is unimportant.

- 3) The term D becomes the dominant forcing north of about 40°N, as can be seen from the similarity of F and A (i.e., $|N| \ll |F|$) in that region for each of the simulations.
- 4) The term N in Historical1 cools and opposes warming from the ocean circulation D in the region of strong positive SST anomalies surrounding the southern tip of Greenland. Internal AMV SST is strongly forced by D here.
- 5) North of 30°N, D in IE0–30 is small compared with D in IEAll or IE30–60. This is consistent with D in the IE primarily being forced by the weather noise there with little contribution from unforced ocean dynamics. The forcing could be through any of the weather noise forcings: heat, wind stress, or freshwater flux. Chen et al. (2016) found that a warm SST band in the AMV pattern of CCSM3 at about 40°–45°N in the western and central Atlantic is forced by the ocean dynamics response to the weather noise wind stress, while the warm SST to the east of that band is forced by the weather noise heat flux.
- 6) The internal AMV SST response north of 30°N in IE0–30N involves D , as in that region $N = 0$ by construction, but $\text{SST} \neq 0$ and $D \neq 0$. However, atmospheric teleconnections, through a nonlocal response of F to the lower-latitude SST, could also be playing a role.

5. Conclusions

The paper evaluates the roles of weather noise forcing and ocean dynamics in explaining North Atlantic multidecadal SST variability related to the AMV index in a coupled GCM simulation with historical external forcing. The main issue is to examine if weather noise forcing is a viable mechanism for producing AMV. The results indicate that weather noise forcing plays an important but secondary role.

The experimental design of this study extends that of Chen et al. (2016) to include historical external forcing and the evaluation of the roles of noise forcing applied separately in the southern and northern portions of the AMV region, defined in this study as the North Atlantic from the equator to 60°N. Results presented here are consistent with the earlier results. Adding time-varying external forcing and restricting the simulations to the historical period highlights issues of attribution of AMV that arise in analysis of observed data with its small sample of AMV events. New results are that detrended external and internally forced AMV variability have approximately the same magnitude, and that AMV in the subtropical gyre has a substantial contribution from forcing by the atmospheric weather noise

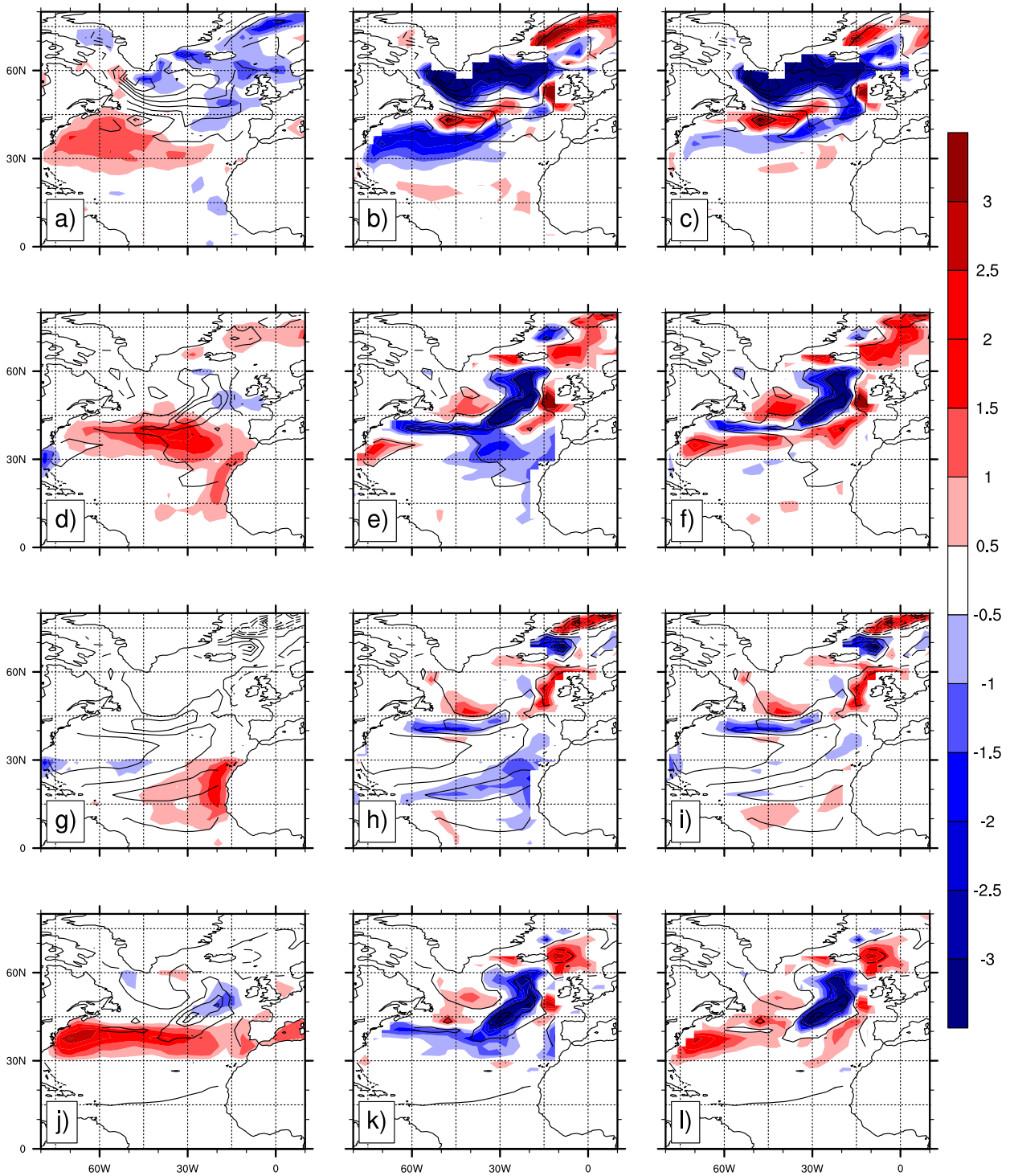


FIG. 13. Simultaneous regressions of standardized internal AMV indices against the terms of the equilibrium heat budget [Eq. (4)]. Internal surface heat budget components (shading; $W m^{-2}$ per standard deviation) and SST (contours; $^{\circ}C$ per standard deviation) are plotted. Rows are for AMV index and 11-yr running mean internal heat flux by case: (a)–(c) Historical1, (d)–(f) IEAll, (g)–(i) IE0–30N, and (j)–(l) IE30–60N. Columns are heat fluxes: (left) weather noise N , (center) feedback F , and (right) ocean dynamics D ; $F = D - N$ in each row.

while ocean dynamics not produced by weather noise forcing is predominant in the subpolar gyre. The internal AMV index forced by weather noise in the subtropical gyre is distinct from the internal AMV index forced by weather noise in the subpolar gyre, and the contributions from the two regions are about equal in producing the overall weather noise forced contribution to the internal AMV index. There is large variability of the internal AMOC/internal AMV relationship between century-length historical simulations, but the relationship is consistent with [Chen et al. \(2016\)](#) when averaged over the full Historical ensemble.

Weather noise forcing can explain about 10% of the variance of the CGCM internal AMV index, a value marginally significantly different from zero. The results from a quasi-equilibrium energy budget analysis indicate that weather noise forcing plays an important role in forcing internal AMV SST pattern in the southern part of the AMV region (0° – 30° N). There, the weather noise heat flux provides the most important forcing, with little local influence from ocean dynamics. In the middle part of the AMV region (30° – 50° N), ocean dynamics is more important than the weather noise heat flux, but the ocean dynamics contribution is primarily weather noise forced. The structure of the internal AMV SST variability in this region has a characteristic banded structure similar to that found by [Chen et al. \(2016\)](#) and attributed to forcing by the wind stress component of the weather noise. The internal AMV SST variability in the far northern part of the AMV region dominates the AMV structure, and also contributes a longer centennial time scale to the AMV index, but is not primarily weather noise forced. This part of the pattern has to be attributed to ocean internal variability, possibly coupled to atmospheric and sea ice feedbacks, subject to concerns about the biases in the diagnostic procedures.

The diagnosis of the internal AMV variability in the historical simulation employed a suite of diagnostic models and procedures, including an ensemble of historically forced CGCM simulations, used to estimate the externally forced component; an ensemble of SST and externally forced AGCM simulations, used to estimate the weather noise surface fluxes; and a set of diagnostic interactive ensemble CGCM simulations, used to isolate the coupled response to the weather noise forcing surface fluxes of the historical simulation. It was found that the contribution of ocean dynamics not forced by the weather noise was small in the internal AMV of the weather noise forced diagnostic simulations. This result allows the weather noise forced contributions of ocean dynamics to be estimated, but also indicates that interactive ensemble simulations are

deficient in the contribution from unforced ocean dynamics.

Major uncertainties in the results are due to the small size of the CGCM ensemble and the biases in the interactive ensemble version CGCM relative to the CGCM. The interactive ensemble biases, including large warm surface temperature biases in the northern part of the North Atlantic, are due to unphysical aspects of the coupling between the atmospheric ensemble and the land and sea ice models intrinsic to the architecture of the coupler. These were dealt with by a postprocessing bias correction procedure that, while partially successful, has some drawbacks. The contribution of residual noise due to the use of small ensembles in the separate parts of the procedures to the explained variance was estimated, and this estimate can be verified using larger ensembles. However, the most serious issue with the diagnosis is that coupling problems in the interactive ensemble, especially those affecting sea ice, probably distort the coupled atmosphere–ocean–sea ice dynamics in a sensitive part of the North Atlantic.

With regard to the Clement/Zhang controversy concerning the roles of weather noise and ocean dynamics in AMV, we assumed an equilibrium heat budget balancing the net atmospheric surface heat flux and the ocean dynamics contribution, and regressed the terms of the heat budget against the AMV indices in various simulations. We found that the primary heat balance in the subpolar gyre was between ocean-dynamics-forced and SST-forced heat fluxes (potentially predictable), while the balance was between weather-noise-forced and SST-forced heat fluxes in the subtropical gyre (growth not predictable).

Acknowledgments. We gratefully acknowledge the assistance of Ben Kirtman and Dughong Min, who provided us with and supported their CCSM3 interactive ensemble code, modified to include the provision for adding specified fields to the surface fluxes provided to the ocean. We thank the anonymous reviewers for their constructive and insightful comments and recommendations. The contributions of Colfescu were supported by the National Centre for Atmospheric Science (NCAS). The contributions of Colfescu and Schneider were supported by NSF Grants ATM-0653123, AGS 1558821, and ATM-1137902. Schneider was also supported by NSF Grant AGS 1338427, NOAA Grant NA14OAR4310160, and NASA Grant NNX14AM19G. The NCAR CISL and NASA Advanced Super Computer Division provided computer resources for the simulations. Data analyses and plotting were done using NCL and GrADS.

APPENDIX A

Decomposition of a Variable: CGCM

The decomposition of the solution for any variable $T_{\text{Historical1}}$ from Historical1 follows [Colfescu et al. \(2013\)](#):

$$T_{\text{Historical1}} = T^{\text{Ext}} + T_{\text{Historical1}}^{\text{Int}}. \quad (\text{A1})$$

The externally forced component T^{Ext} is taken to be the ensemble mean of the T values from the CCSM3 ensemble, in this case with five ensemble members $T_{\text{Historical}(i)}$,

$$T^{\text{Ext}} = \frac{1}{5} \sum_{(i)=1}^{(i)=5} T_{\text{Historical}(i)}. \quad (\text{A2})$$

The internally generated component $T_{\text{Historical1}}^{\text{Int}}$ is then the Historical1 solution minus the externally forced component,

$$T_{\text{Historical1}}^{\text{Int}} = T_{\text{Historical1}} - T^{\text{Ext}}. \quad (\text{A3})$$

The internal component can be separated into the weather-noise-forced part $T_{\text{Historical1}}^{\text{Int WeaNoise}}$ and that due to other sources $T_{\text{Historical1}}^{\text{Int Other}}$,

$$T_{\text{Historical1}}^{\text{Int}} = T_{\text{Historical1}}^{\text{Int WeaNoise}} + T_{\text{Historical1}}^{\text{Int Other}}, \quad (\text{A4})$$

where $T_{\text{Historical1}}^{\text{Int WeaNoise}}$ is to be estimated using IE simulations. Once $T_{\text{Historical1}}^{\text{Int WeaNoise}}$ is determined, $T_{\text{Historical1}}^{\text{Int Other}}$ can be found as a residual from $T_{\text{Historical1}}^{\text{Int}}$ using Eq. (A4). In discussing the CGCM results, those found from Eq. (A2) will be called ‘‘Historical external’’ and those from Eq. (A3) called ‘‘Historical1 internal.’’

APPENDIX B

Decomposition of a Variable: Interactive Ensemble

A similar decomposition is applied for a given variable $T_{\text{IE}x}$ in an interactive ensemble simulation, where x refers to the different experiment names. For the five IE experiments described in this paper,

$$T_{\text{IEAll}} = T_{\text{IE}}^{\text{Ext}} + T_{\text{IEAll}}^{\text{Int}} + T_{\text{IE}}^{\text{Bias}}, \quad (\text{B1a})$$

$$T_{\text{IENoNoise}} = T_{\text{IE}}^{\text{Ext}} + T_{\text{IENoNoise}}^{\text{Int}} + T_{\text{IE}}^{\text{Bias}}, \quad (\text{B1b})$$

$$T_{\text{IENoHistorical}} = T_{\text{IENoHistorical}}^{\text{Int}} + T_{\text{IE}}^{\text{Bias}}, \quad (\text{B1c})$$

$$T_{\text{IE0-30N}}^{\text{Int}} = T_{\text{IE0-30N}}^{\text{Int}} + T_{\text{IE}}^{\text{Bias}}, \quad \text{and} \quad (\text{B1d})$$

$$T_{\text{IE30-60N}} = T_{\text{IE30-60N}}^{\text{Int}} + T_{\text{IE}}^{\text{Bias}}, \quad (\text{B1e})$$

where the external component $T_{\text{IE}}^{\text{Ext}}$ is the IE response to the external forcing, and internal variability is represented by $T_{\text{IE}x}^{\text{Int}}$. Since IENoHistorical uses constant preindustrial external forcing, $T_{\text{IE}}^{\text{Ext}}$ is not included in Eq. (B1c). The bias term $T_{\text{IE}}^{\text{Bias}}$ represents a time-dependent climate drift in the IE, probably resulting from the use of ocean initial conditions taken from the equilibrated preindustrial CCSM3 run that are not in balance in the IE climate. The bias term is taken to be the same in each IE simulation, since they each share the same ocean initial state and the same biased physics.

The internal component is decomposed into weather noise forced and other components as in Eq. (A4):

$$T_{\text{IE}x}^{\text{Int}} = T_{\text{Historical1}}^{\text{Int WeaNoise}} + T_{\text{IE}x}^{\text{Int Other}}, \quad (\text{B2})$$

where the term representing internal variability forced by the weather noise $T_{\text{Historical1}}^{\text{Int WeaNoise}}$ is taken to be the same as the decomposition of Historical1, and is not included in the decomposition Eq. (B1b) for IENoNoise. Then Eqs. (B1a–c) and (B2) give

$$T_{\text{Historical1}}^{\text{Int WeaNoise}} = T_{\text{IEAll}}^{\text{Int}} - T_{\text{IENoNoise}}^{\text{Int}} + T_{\text{IENoNoise}}^{\text{Int Other}} - T_{\text{IEAll}}^{\text{Int Other}}, \quad (\text{B3a})$$

$$T_{\text{IE}}^{\text{Ext}} = T_{\text{IEAll}}^{\text{Ext}} - T_{\text{IENoHistorical}}^{\text{Ext}} + T_{\text{IENoHistorical}}^{\text{Int Other}} - T_{\text{IEAll}}^{\text{Int Other}}, \quad \text{and} \quad (\text{B3b})$$

$$T_{\text{IE}}^{\text{Bias}} = T_{\text{IENoNoise}}^{\text{Bias}} - T_{\text{IEAll}}^{\text{Bias}} + T_{\text{IENoHistorical}}^{\text{Bias}} - T_{\text{IENoHistorical}}^{\text{Int Other}} - T_{\text{IENoNoise}}^{\text{Int Other}}. \quad (\text{B3c})$$

A bias correction is applied to estimate the internal component of variables forced by the regionally restricted weather noise in simulations IE0–30N and IE30–60N:

$$T_{\text{IE0-30N}}^{\text{Int WeaNoise}} = T_{\text{IE0-30N}}^{\text{Int}} - T_{\text{IENoNoise}}^{\text{Int}} + T_{\text{IENoNoise}}^{\text{Int Other}} - T_{\text{IE0-30N}}^{\text{Int Other}}, \quad (\text{B3d})$$

$$T_{\text{IE30-60N}}^{\text{Int WeaNoise}} = T_{\text{IE30-60N}}^{\text{Int}} - T_{\text{IENoNoise}}^{\text{Int}} + T_{\text{IENoNoise}}^{\text{Int Other}} - T_{\text{IE30-60N}}^{\text{Int Other}}. \quad (\text{B3e})$$

The total bias-corrected solutions are obtained by adding the bias-corrected internal and external components, which is equivalent to subtracting the bias from the individual IE simulations in Eqs. (B1a), (B1d), and (B1e).

The Int Other variability remains in our decomposition of the Historical or IE simulations and is

different for each simulation. Therefore, it is not possible to completely decompose the internal variability in either the Historical or IE simulation into Int WeaNoise and Int Other components. Consequently, the Int Other terms are not taken into account in the bias correction. That is, the Int Other contributions remain as a source of error in what we call the “bias-corrected” components. Using subscript BC to represent our partial bias corrections that are applied to the results reported in this paper:

$$(T_{\text{Historical1}}^{\text{Int WeaNoise}})_{\text{BC}} = T_{\text{IEAll}} - T_{\text{IENoNoise}} = T_{\text{Historical1}}^{\text{Int WeaNoise}} - T_{\text{IENoNoise}}^{\text{Int Other}} + T_{\text{IEAll}}^{\text{Int Other}}, \quad (\text{B4a})$$

$$(T_{\text{IE}}^{\text{Ext}})_{\text{BC}} = T_{\text{IEAll}} - T_{\text{IENoHistorical}} = T_{\text{IE}}^{\text{Ext}} - T_{\text{IENoHistorical}}^{\text{Int Other}} + T_{\text{IEAll}}^{\text{Int Other}}, \quad (\text{B4b})$$

$$(T_{\text{IE}}^{\text{Bias}})_{\text{BC}} = T_{\text{IENoNoise}} - T_{\text{IEAll}} + T_{\text{IENoHistorical}} = T_{\text{IE}}^{\text{Bias}} - T_{\text{IENoHistorical}}^{\text{Int Other}} - T_{\text{IENoNoise}}^{\text{Int Other}}, \quad (\text{B4c})$$

$$(T_{\text{IE0-30N}}^{\text{Int WeaNoise}})_{\text{BC}} = T_{\text{IE0-30N}} - T_{\text{IENoNoise}} = T_{\text{IE0-30N}}^{\text{Int WeaNoise}} - T_{\text{IENoNoise}}^{\text{Int Other}} - T_{\text{IE0-30N}}^{\text{Int Other}}, \quad \text{and} \quad (\text{B4d})$$

$$(T_{\text{IE30-60N}}^{\text{Int WeaNoise}})_{\text{BC}} = T_{\text{IE30-60N}} - T_{\text{IENoNoise}} = T_{\text{IE30-60N}}^{\text{Int WeaNoise}} - T_{\text{IENoNoise}}^{\text{Int Other}} + T_{\text{IE30-60N}}^{\text{Int Other}}. \quad (\text{B4e})$$

The Int Other variability can arise from physical processes not forced by the weather noise, particularly ocean internal variability (Wu et al. 2004) or processes involving ocean dynamics coupled to atmospheric feedbacks to SST and/or sea ice anomalies. An important nonphysical source of Int Other variability is errors in the decomposition into forced and noise components due to the ensembles, the five-member CGCM ensemble and the six-member AGCM ensembles, used in several places in the process. The nonphysical source Int Other variability can be effectively eliminated by the use of large enough ensembles, while reducing the physical source could be accomplished using ensembles of IE simulations with the same weather noise and external forcing or by replacing the IE ocean component with an ocean model ensemble (Kirtman et al. 2006).

The external component given by the bias correction procedure above should be low-pass filtered (e.g., leaving decadal and longer time scales) when the

atmospheric ensemble is small, since the bias correction adds high-frequency numerical noise from the IE AGCM ensemble to the external as well as the internal variability. In the six-AGCM IE setup used in this study, the explained variance of monthly unfiltered data between Historical1 and IEAll is reduced from values close to 0.9 for the uncorrected data to less than 0.2 for total, external, and internal components after bias correction using the unfiltered external component. Changes in explained variance between uncorrected and bias-corrected multidecadal results are on the order of 0.1.

APPENDIX C

Explained Variance: Estimation of Noise Effects due to the Use of Small Ensembles and Bias Correction

The explained variance E quantifies the fractional variance of a time series Y “explained” by linear regression against X , another time series, with residual N : $Y = aX + N$. Using brackets $\langle \rangle$ to represent the covariance operator,

$$E(X, Y) = \frac{\langle XY \rangle^2}{\langle X^2 \rangle \langle Y^2 \rangle}. \quad (\text{C1})$$

The explained variance is the square of the correlation between X and Y .

a. Explained variances of external and internal components

The explained variances of the total by the internal and external components, for example as given in Eq. (A3), do not necessarily add to one, except when the covariance between the internal and external components is zero. Representing the decomposition as $c = a + b$, where c is the total, a is the external component, and b is the internal component:

$$E(c, a) + E(c, b) = \frac{\langle ca \rangle^2}{\langle c^2 \rangle \langle a^2 \rangle} + \frac{\langle cb \rangle^2}{\langle c^2 \rangle \langle b^2 \rangle} = 1 + \frac{\langle ab \rangle}{\langle c^2 \rangle} \left[2 + \langle ab \rangle \left(\frac{\langle a^2 \rangle + \langle b^2 \rangle}{\langle a^2 \rangle \langle b^2 \rangle} \right) \right]. \quad (\text{C2})$$

If $\langle ab \rangle = 0$, then $E(c, a) + E(c, b) = 1$. If $\langle ab \rangle \neq 0$, then the rhs in Eq. (C2) is not equal to 1 except for the special case $2 + \langle ab \rangle [(\langle a^2 \rangle + \langle b^2 \rangle) / (\langle a^2 \rangle \langle b^2 \rangle)] = 0$. If $\langle ab \rangle$ is positive, $E(c, a) + E(c, b) > 1$. The sum of

the external and internal explained variances thus contains information about the degree of dependence between the internal and external components.

b. Ensembling-adjusted explained variance

Explained variance is a useful metric for quantifying and removing the contributions of residual noise sources introduced through the use of small ensembles. The approach described below extends that of [Chen et al. \(2013\)](#); see their online supplemental material). The numbers of ensemble members in the five-member CCSM3, six-member IE atmospheric component, and six-member AGCM ensembles are small, so that ensemble means, and especially the internal variability, weather noise, and IE responses to the weather noise contain substantial errors in the form of “ensembling noise” (to distinguish from the physically based “weather noise”). Ensembling noise is generated in the estimate of the external and internal components of Historical1, in the estimate of the Historical1 weather noise, in the response of the atmospheric ensemble to the SST in the IE, and in the bias correction.

If the X and Y time series have ensembling noise that is known to contribute zero covariance to the numerator of E , the maximum value that E can attain can be reduced a priori from 1 to $E_{MAX} < 1$. Here we estimate E_{MAX} for internal variability in two cases that are applied to our analysis. The quantity E_p , which will be called the “ensembling-adjusted explained variance,” is defined as the explained variance relative to E_{MAX} :

$$E_p = \frac{E}{E_{MAX}}. \tag{C3}$$

The ensembling-adjusted explained variance is meant to approximate the explained variance by processes remaining after removal of the residual noise and clarifies the attribution of internal variability to weather noise forcing and other physical process.

The calculation of E_{MAX} begins with decomposing X and Y into residual-noise-removed components X_p , Y_p , and residual noise N_X , N_Y :

$$X = X_p + N_X, \tag{C4}$$

$$Y = Y_p + N_Y. \tag{C5}$$

Assuming that $\langle YN_X \rangle = \langle XN_Y \rangle = \langle N_XN_Y \rangle = 0$,

$$E = \frac{\langle X_p Y_p \rangle^2}{\langle X^2 \rangle \langle Y^2 \rangle}. \tag{C6}$$

An upper bound for E is then E_{MAX} ,

$$E_{MAX} = \frac{\langle X_p^2 \rangle \langle Y_p^2 \rangle}{\langle X^2 \rangle \langle Y^2 \rangle}, \tag{C7}$$

and $0 < E < E_{MAX}$ since E/E_{MAX} is the explained variance of X_p and Y_p . To obtain estimates for E_{MAX} it is also assumed that $\langle YN_Y \rangle = \langle XN_X \rangle$. If nothing is known about the properties of the residual noise, $E_{MAX} = 1$.

The value of E_{MAX} depends on what quantities X and Y represent. First the decomposition of X and Y is carried out for internal variability in Historical1, for the weather noise inferred from Historical1, and for the bias-corrected interactive ensemble. Then E_{MAX} is estimated for two situations: 1) Y is the Historical1 internal component and X is the internal component from a weather-noise-forced IE simulation; 2) Y is the IEAll internal component and X is the internal component from IE0–30N or from IE30–60N.

Historical1 internal component Y is decomposed into component Y_p that includes all of the physical processes, and a residual noise component arising from the small size of the Historical ensemble. Each Historical ensemble member can be decomposed into the true external component \bar{H} and the true internal component H'_i :

$$H_i = \bar{H} + H'_i. \tag{C8}$$

The estimated internal component obtained from the Historical ensemble is

$$Y = H_1 - \frac{1}{5} \sum_{i=1}^5 H_i. \tag{C9}$$

Substituting in Eq. (C9) from Eq. (C8)

$$Y = \frac{4}{5} H'_1 - \frac{1}{5} \sum_{i=2}^5 H'_i. \tag{C10}$$

The internal component from of any member of the Historical ensemble except for Historical1 will have zero covariance with the internal component of any IE simulation. Therefore, $Y_p = (4/5)H'_1$ and $N_Y = -(1/5)\sum_{i=2}^5 H'_i$. The variance of the internal component of each ensemble member is taken to be the same, $\langle H_i'^2 \rangle = \langle H_1'^2 \rangle$, so that

$$\langle Y_p^2 \rangle = \frac{16}{25} \langle H_1'^2 \rangle, \tag{C11}$$

$$\langle Y^2 \rangle = \frac{4}{5} \langle H_1^2 \rangle. \quad (\text{C12})$$

The residual noise in the small CGCM ensemble together with the choice of using the full Historical ensemble to estimate the external component contributes a factor of $\langle Y_P^2 \rangle / \langle Y^2 \rangle = 0.8$ to E_{MAX} . If the estimate of the external component uses the mean of Historical2–Historical5, so that the error is independent from Historical1 internal, the contribution to E_{MAX} is the same.

Next, the weather noise, denoted X^W , is decomposed. Using A for the atmospheric model variable,

$$X^W = X_P^W + N_{(X^W)} = H_1 - \frac{1}{6} \sum_{i=1}^6 A_i, \quad (\text{C13})$$

$$A_i = \bar{H} + A'_i, \quad (\text{C14})$$

since the SST and externally forced response of the atmospheric model in Historical1 and the AGCM forced by the Historical1 SST is taken to be the same. Then $X_P^W = H_1$ and $N_{(X^W)} = -(1/6) \sum_{i=1}^6 A'_i$. Taking $\langle A_i^2 \rangle = \langle H_1^2 \rangle$ gives the contributions of the true weather noise and ensemble-generated noise to the estimated weather noise:

$$\langle (X_P^W)^2 \rangle = \langle H_1^2 \rangle, \quad (\text{C15})$$

$$\langle (X^W)^2 \rangle = \frac{7}{6} \langle H_1^2 \rangle. \quad (\text{C16})$$

The weather-noise-forced, bias-corrected interactive ensemble internal component, designated as X , is composed of four components:

$$X = F_W + N_W + N_A + N_B, \quad (\text{C17})$$

where F_W is the component forced by the true weather noise X^W , N_W is the component forced by the error in the weather noise $N_{(X^W)}$, N_A is the residual noise from the IE atmospheric ensemble, and N_B is the residual noise from the IENoNoise simulation used in the bias correction. Each of the terms on the rhs of Eq. (C17) is uncorrelated with any of the other terms, since each is noise generated from a different process. Then the variance of X is the sum of the variances of the four terms on the rhs of Eq. (C17).

The maximum response to the true weather noise of Historical1 is

$$\langle (F_W)^2 \rangle = \langle H_1^2 \rangle. \quad (\text{C18})$$

The response to the residual noise from the six-member AGCM ensemble in the estimation of the Historical1 weather noise is

$$\langle (N_W)^2 \rangle = \frac{1}{6} \langle H_1^2 \rangle. \quad (\text{C19})$$

The contribution from the residual noise forcing in the six-member IE atmospheric model ensemble is

$$\langle (N_A)^2 \rangle = \frac{1}{6} \langle H_1^2 \rangle. \quad (\text{C20})$$

The residual noise contribution from the six-member atmospheric model ensemble in the IENoNoise simulation in the bias correction is

$$\langle (N_B)^2 \rangle = \frac{1}{6} \langle H_1^2 \rangle. \quad (\text{C21})$$

Then the total variance of X is

$$\langle X^2 \rangle = \frac{3}{2} \langle H_1^2 \rangle. \quad (\text{C22})$$

The estimates of E_{MAX} for various cases can be made as follows.

- 1) CASE 1: Y IS HISTORICAL1, X IS IEALL, IE0–30N, OR IE30–60N

In the regions where the weather noise forcing is applied $X_P = F_W$ and is zero elsewhere. Then $\langle X_P^2 \rangle / \langle X^2 \rangle = 2/3$. Using this along with Eqs. (C11) and (C12) in Eq. (C7) gives $E_{\text{MAX}} = 8/15 = 0.53$ in the regions where the weather noise forcing is applied, and zero elsewhere. We use $E_{\text{MAX}} = 0.53$ everywhere to account for possible teleconnections in calculating E_P .

- 2) CASE 2: Y IS IEALL, X IS IE0–30N OR IE30–60N

In this case, X and Y are both IE simulations. The same estimated weather noise forcing, $F_W + N_W$, is applied in each case, and the same residual noise N_B is used for all bias correction. The residual noise from the weather noise estimation and the bias correction both contribute to the covariance $\langle XY \rangle$ in the explained variance. Then $X_P = Y_P = F_W + N_W + N_B$ in regions of common noise forcing, and $\langle X_P^2 \rangle = \langle Y_P^2 \rangle = (4/3) \langle H_1^2 \rangle$. Using $\langle X^2 \rangle = \langle Y^2 \rangle$ and Eq. (C22), $E_{\text{MAX}} = 64/81 = 0.79$ in common forcing regions. Taking $F_W = N_W = 0$ for the regional simulations, the background explained variance between IEAll and IE0–30N or IE30–60N in regions where the noise forcing is zero is estimated to be 0.05, due to the common bias correction.

REFERENCES

- Barsugli, J. J., and D. S. Battisti, 1998: The basic effects of atmosphere–ocean thermal coupling on midlatitude variability.

- J. Atmos. Sci.*, **55**, 477–493, [https://doi.org/10.1175/1520-0469\(1998\)055<0477:TBEAOA>2.0.CO;2](https://doi.org/10.1175/1520-0469(1998)055<0477:TBEAOA>2.0.CO;2).
- Bellomo, K., L. N. Murphy, M. A. Cane, A. C. Clement, and L. M. Polvani, 2018: Historical forcings as main drivers of the Atlantic multidecadal variability in the CESM large ensemble. *Climate Dyn.*, **50**, 3687–3698, <https://doi.org/10.1007/s00382-017-3834-3>.
- Bjerknes, J., 1964: Atlantic air–sea interaction. *Advances in Geophysics*, Vol. 10, Academic Press, 1–82, [https://doi.org/10.1016/S0065-2687\(08\)60005-9](https://doi.org/10.1016/S0065-2687(08)60005-9).
- Bombardi, R., and Coauthors, 2015: Evaluation of the CFSv2 CMIP5 decadal predictions. *Climate Dyn.*, **44**, 543–557, <https://doi.org/10.1007/s00382-014-2360-9>.
- Booth, B. B. B., N. J. Dunstone, P. R. Halloran, T. Andrews, and N. Bellouin, 2012: Aerosols implicated as a prime driver of twentieth-century North Atlantic climate variability. *Nature*, **484**, 228–232, <https://doi.org/10.1038/nature10946>.
- Bretherton, C. S., and D. S. Battisti, 2000: An interpretation of the results from atmospheric general circulation models forced by the time history of the observed sea surface temperature distribution. *Geophys. Res. Lett.*, **27**, 767–770, <https://doi.org/10.1029/1999GL010910>.
- Bryan, K., and F. C. Hansen, 1995: A stochastic model of North Atlantic climate variability on a decade to century time-scale. *Proc. Workshop on Decade-to-Century Time Scales of Climate Variability*, Irvine, CA, National Research Council Board on Atmospheric Sciences and Climate, National Academy of Sciences, 363–364.
- Buckley, M. W., and J. Marshall, 2016: Observations, inferences, and mechanisms of the Atlantic meridional overturning circulation: A review. *Rev. Geophys.*, **54**, 5–63, <https://doi.org/10.1002/2015RG000493>.
- Chen, H., E. K. Schneider, B. P. Kirtman, and I. Colfescu, 2013: Evaluation of weather noise and its role in climate model simulations. *J. Climate*, **26**, 3766–3784, <https://doi.org/10.1175/JCLI-D-12-00292.1>.
- , —, and Z. Wu, 2016: Mechanisms of internally generated decadal-to-multidecadal variability of SST in the Atlantic Ocean in a coupled GCM. *Climate Dyn.*, **46**, 1517–1546, <https://doi.org/10.1007/s00382-015-2660-8>.
- Clement, A., K. Bellomo, L. N. Murphy, M. A. Cane, T. Mauritsen, G. Radel, and B. Stevens, 2015: The Atlantic multidecadal oscillation without a role for ocean circulation. *Science*, **350**, 320–324, <https://doi.org/10.1126/science.aab3980>.
- , M. A. Cane, L. N. Murphy, K. Bellomo, T. Mauritsen, and B. Stevens, 2016: Response to comment on “The Atlantic multidecadal oscillation without a role for ocean circulation.” *Science*, **352**, 1527, <https://doi.org/10.1126/science.aaf2575>.
- Colfescu, I., and E. K. Schneider, 2017: Internal atmospheric noise characteristics in twentieth century coupled atmosphere–ocean model simulations. *Climate Dyn.*, **49**, 2205–2217, <https://doi.org/10.1007/s00382-016-3440-9>.
- , —, and H. Chen, 2013: Consistency of 20th century sea level pressure trends as simulated by a coupled and uncoupled GCM. *Geophys. Res. Lett.*, **40**, 3276–3280, <https://doi.org/10.1002/grl.50545>.
- Collins, W. D., and Coauthors, 2006a: The Community Climate System Model version 3 (CCSM3). *J. Climate*, **19**, 2122–2143, <https://doi.org/10.1175/JCLI3761.1>.
- , and Coauthors, 2006b: The formulation and atmospheric simulation of the Community Atmosphere Model version 3 (CAM3). *J. Climate*, **19**, 2144–2161, <https://doi.org/10.1175/JCLI3760.1>.
- Delworth, T. L., 1996: North Atlantic interannual variability in a coupled ocean–atmosphere model. *J. Climate*, **9**, 2356–2375, [https://doi.org/10.1175/1520-0442\(1996\)009<2356:NAIVIA>2.0.CO;2](https://doi.org/10.1175/1520-0442(1996)009<2356:NAIVIA>2.0.CO;2).
- , and R. J. Greatbatch, 2000: Multidecadal thermohaline circulation variability driven by atmospheric surface flux forcing. *J. Climate*, **13**, 1481–1495, [https://doi.org/10.1175/1520-0442\(2000\)013<1481:MTCVDB>2.0.CO;2](https://doi.org/10.1175/1520-0442(2000)013<1481:MTCVDB>2.0.CO;2).
- , and M. E. Mann, 2000: Observed and simulated multidecadal variability in the Northern Hemisphere. *Climate Dyn.*, **16**, 661–676, <https://doi.org/10.1007/s003820000075>.
- , R. Zhang, and M. E. Mann, 2007: Decadal to centennial variability of the Atlantic from observations and models. *Ocean Circulation: Mechanisms and Impacts*, *Geophys. Monogr.*, Vol. 173, Amer. Geophys. Union, 131–148.
- Deser, C., and M. L. Blackmon, 1993: Surface climate variations over the North Atlantic Ocean during winter: 1900–1989. *J. Climate*, **6**, 1743–1753, [https://doi.org/10.1175/1520-0442\(1993\)006<1743:SCVOTN>2.0.CO;2](https://doi.org/10.1175/1520-0442(1993)006<1743:SCVOTN>2.0.CO;2).
- , G. Magnusdottir, R. Saravanan, and A. Phillips, 2004: The effects of North Atlantic SST and sea ice anomalies on the winter circulation in CCM3. Part II: Direct and indirect components of the response. *J. Climate*, **17**, 877–889, [https://doi.org/10.1175/1520-0442\(2004\)017<0877:TEONAS>2.0.CO;2](https://doi.org/10.1175/1520-0442(2004)017<0877:TEONAS>2.0.CO;2).
- Eade, R., D. Smith, A. Scaife, E. Wallace, N. Dunstone, L. Hermanson, and N. Robinson, 2014: Do seasonal-to-decadal climate predictions underestimate the predictability of the real world? *Geophys. Res. Lett.*, **41**, 5620–5628, <https://doi.org/10.1002/2014GL061146>.
- Enfield, D. B., A. M. Mestas-Núñez, and P. J. Trimble, 2001: The Atlantic multidecadal oscillation and its relation to rainfall and river flows in the continental U.S. *Geophys. Res. Lett.*, **28**, 2077–2080, <https://doi.org/10.1029/2000GL012745>.
- Griffies, S. H., and E. Tziperman, 1995: A linear thermohaline oscillator driven by stochastic atmospheric forcing. *J. Climate*, **8**, 2440–2453, [https://doi.org/10.1175/1520-0442\(1995\)008<2440:ALTODB>2.0.CO;2](https://doi.org/10.1175/1520-0442(1995)008<2440:ALTODB>2.0.CO;2).
- , and K. Bryan, 1997a: Predictability of North Atlantic multidecadal climate variability. *Science*, **275**, 181–184, <https://doi.org/10.1126/science.275.5297.181>.
- , and —, 1997b: A predictability study of simulated North Atlantic multidecadal variability. *Climate Dyn.*, **13**, 459–487, <https://doi.org/10.1007/s003820050177>.
- Gulev, S. K., M. Latif, N. Keenlyside, W. Park, and K. P. Koltermann, 2013: North Atlantic Ocean control on surface heat flux on multidecadal timescales. *Nature*, **499**, 464–467, <https://doi.org/10.1038/nature12268>.
- Häkkinen, S., P. Rhines, and D. Worthen, 2011: Atmospheric blocking and Atlantic multidecadal ocean variability. *Science*, **334**, 655–659, <https://doi.org/10.1126/science.1205683>.
- , —, and —, 2013: Northern North Atlantic sea surface height and ocean heat content variability. *J. Geophys. Res. Oceans*, **118**, 3670–3678, <https://doi.org/10.1002/jgrc.20268>.
- Hasselmann, K., 1976: Stochastic climate models Part I. Theory. *Tellus*, **28**, 473–485, <https://doi.org/10.3402/tellusa.v28i6.11316>.
- Kirtman, B. P., and J. Shukla, 2002: Interactive coupled ensemble: A new coupling strategy for CGCMs. *Geophys. Res. Lett.*, **29**, 1367, <https://doi.org/10.1029/2002GL014834>.
- , K. Pegion, and S. Kinter, 2005: Internal atmospheric dynamics and tropical Indo-Pacific climate variability. *J. Atmos. Sci.*, **62**, 2220–2233, <https://doi.org/10.1175/JAS3449.1>.
- , R. Wu, and S.-W. Yeh, 2006: Internal ocean dynamics and climate variability. COLA Tech. Rep. 225, 44 pp.

- , D. M. Straus, D. Min, E. K. Schneider, and L. Siqueira, 2009: Toward linking weather and climate in the interactive ensemble NCAR climate model. *Geophys. Res. Lett.*, **36**, L13705, <https://doi.org/10.1029/2009GL038389>.
- , E. K. Schneider, D. M. Straus, D. Min, and R. Burgman, 2011: How weather impacts the forced climate response. *Climate Dyn.*, **37**, 2389–2416, <https://doi.org/10.1007/s00382-011-1084-3>.
- Knight, J. R., C. K. Folland, and A. A. Scaife, 2006: Climate impacts of the Atlantic multidecadal oscillation. *Geophys. Res. Lett.*, **33**, L17706, <https://doi.org/10.1029/2006GL026242>.
- Kushnir, Y., and I. M. Held, 1996: Equilibrium atmospheric response to North Atlantic SST anomalies. *J. Climate*, **9**, 1208–1220, [https://doi.org/10.1175/1520-0442\(1996\)009<1208:EARTNA>2.0.CO;2](https://doi.org/10.1175/1520-0442(1996)009<1208:EARTNA>2.0.CO;2).
- Latif, M., and Coauthors, 2004: Reconstructing, monitoring, and predicting multidecadal-scale changes in the North Atlantic thermohaline circulation with sea surface temperature. *J. Climate*, **17**, 1605–1614, [https://doi.org/10.1175/1520-0442\(2004\)017<1605:RMAPMC>2.0.CO;2](https://doi.org/10.1175/1520-0442(2004)017<1605:RMAPMC>2.0.CO;2).
- Magnusdottir, G., C. Deser, and R. Saravanan, 2004: The effects of North Atlantic SST and sea ice anomalies on the winter circulation in CCM3. Part I: Main features and storm tracks characteristics of the response. *J. Climate*, **17**, 857–876, [https://doi.org/10.1175/1520-0442\(2004\)017<0857:TEONAS>2.0.CO;2](https://doi.org/10.1175/1520-0442(2004)017<0857:TEONAS>2.0.CO;2).
- Mann, M. E., and J. Park, 1996: Joint spatiotemporal modes of surface temperature and sea level pressure variability in the Northern Hemisphere during the last century. *J. Climate*, **9**, 2137–2162, [https://doi.org/10.1175/1520-0442\(1996\)009<2137:JSMOST>2.0.CO;2](https://doi.org/10.1175/1520-0442(1996)009<2137:JSMOST>2.0.CO;2).
- Marini, C., and C. Frankignoul, 2014: An attempt to deconstruct the Atlantic multidecadal oscillation. *Climate Dyn.*, **43**, 607–625, <https://doi.org/10.1007/s00382-013-1852-3>.
- Meehl, G. A., and Coauthors, 2006: Climate change projections for the twenty-first century and climate change commitment in the CCSM3. *J. Climate*, **19**, 2597–2616, <https://doi.org/10.1175/JCLI3746.1>.
- Otterå, O. H., M. Bentsen, H. Drange, and L. Suo, 2010: External forcing as a metronome for Atlantic multidecadal variability. *Nat. Geosci.*, **3**, 688–694, <https://doi.org/10.1038/ngeo955>.
- Park, S., C. Deser, and M. A. Alexander, 2005: Estimation of the surface heat flux response to sea surface temperature anomalies over the global oceans. *J. Climate*, **18**, 4582–4599, <https://doi.org/10.1175/JCLI3521.1>.
- Peings, Y., and G. Magnusdottir, 2014: Forcing of the wintertime atmospheric circulation by the multidecadal fluctuations of the North Atlantic Ocean. *Environ. Res. Lett.*, **9**, 034018, <https://doi.org/10.1088/1748-9326/9/3/034018>.
- Randall, D. A., and Coauthors, 2007: Climate models and their evaluation. *Climate Change 2007: The Physical Science Basis*, S. Solomon et al., Eds., Cambridge University Press, 589–662.
- Schlesinger, M. E., and N. Ramankutty, 1994: An oscillation in the global climate system of period 65–70 years. *Nature*, **367**, 723–726, <https://doi.org/10.1038/367723a0>.
- Schneider, E. K., and J. L. Kinter III, 1994: An examination of internally generated variability in long climate simulations. *Climate Dyn.*, **10**, 181–204, <https://doi.org/10.1007/BF00208987>.
- , and M. Fan, 2007: Weather noise forcing of surface climate variability. *J. Atmos. Sci.*, **64**, 3265–3280, <https://doi.org/10.1175/JAS4026.1>.
- Sutton, R. T., G. D. McCarthy, J. Robson, B. Sinha, A. Archibald, and L. J. Gray, 2018: Atlantic multi-decadal variability and the UK ACSIS programme. *Bull. Amer. Meteor. Soc.*, **99**, 415–425, <https://doi.org/10.1175/BAMS-D-16-0266.1>.
- Ting, M., Y. Kushnir, R. Seager, and C. Li, 2009: Forced and internal twentieth-century SST trends in the North Atlantic. *J. Climate*, **22**, 1469–1481, <https://doi.org/10.1175/2008JCLI2561.1>.
- Trenberth, K. E., and D. J. Shea, 2006: Atlantic hurricanes and natural variability in 2005. *Geophys. Res. Lett.*, **33**, L12704, <https://doi.org/10.1029/2006GL026894>.
- Wu, Z., E. K. Schneider, and B. P. Kirtman, 2004: Causes of low frequency North Atlantic SST variability in a coupled GCM. *Geophys. Res. Lett.*, **31**, L09210, <https://doi.org/10.1029/2004GL019548>.
- Zhang, R., R. Sutton, G. Danabasoglu, T. Delworth, W. M. Kim, J. Robson, and S. J. Yeager, 2016: Comment on “The Atlantic multidecadal oscillation without a role for ocean circulation.” *Science*, **352**, 1527, <https://doi.org/10.1126/science.aaf1660>.